

# Exponential galaxy discs as the quasi-stationary distribution in a Markov chain model simulating stellar scattering

Jian Wu,<sup>1</sup>★ Curtis Struck,<sup>1</sup>★ Bruce G. Elmegreen<sup>2</sup> and Elena D’Onghia<sup>3</sup>

<sup>1</sup>*Department of Physics and Astronomy, Iowa State University, 2323 Osborn Dr., Ames, IA 50011, USA*

<sup>2</sup>*IBM Research Division, T.J. Watson Research Centre, 1101 Kitchawan Road, Yorktown Heights, NY 10598, USA*

<sup>3</sup>*Department of Astronomy, University of Wisconsin-Madison, 475 N Charter St, Madison, WI 53706, USA*

Accepted 2023 April 19. Received 2023 March 21; in original form 2022 November 6

## ABSTRACT

Previous models have shown that stochastic scattering of stars in a two-dimensional galaxy disc can generate a time-independent surface density distribution that is an exponential divided by radius when a constant inward scattering bias is present. Here we show, using a Markov chain model, that similar profiles result from an outward scattering bias, although the disc surface density decreases slowly with time because of a net stellar outflow. The trend towards a near-exponential surface profile is robust, as it exists even if the scattering intensity has moderate radial and time dependences, subject to some limitations on the scattering rates discussed in the text. The exponential scale length of the pseudo-equilibrium disc depends on the scattering bias, the scattering length, and the size of the disc where scattering is important.

**Key words:** galaxies: disc – galaxies: evolution – galaxies: kinematics and dynamics

## 1 INTRODUCTION

The exponential shape of a stellar disc is common in many types of galaxies, such as spirals, dwarf irregulars, and dwarf ellipticals (Borson 1981; Ichikawa et al. 1986; Andredakis et al. 1995; Paterson & Thuan 1996; de Jong 1996; Simard et al. 2011; Herrmann et al. 2013). It is observed at both low and high redshifts (Law et al. 2012; Patrício et al. 2016; Bowler et al. 2017). Even clumpy galaxies with multiple overdense regions in their disc hold an exponential stellar profile (Elmegreen et al. 2005; Bournaud et al. 2007; Shibuya et al. 2016). In spite of the ubiquity of exponential discs, their formation is not well understood.

The emergence of an exponential disc can come from initial and continuing conditions related to cosmic accretion combined with internal processes that shift stars radially in a galaxy. These processes can occur through various mechanisms. Spiral arms produce stellar radial migration near the corotation radius (Sellwood & Binney 2002; Roškar et al. 2008; Vera-Ciro et al. 2014; Daniel & Wyse 2018). Massive clumps in the disc, such as giant molecular clouds, can move stars radially by their gravity when they encounter stars (Elmegreen & Struck 2013; Struck & Elmegreen 2017; Wu et al. 2020). If a galaxy has a central bar, the gravitational force from the bar can modify stellar orbits outside the bar and move the stars radially (Hohl 1971; Debattista et al. 2006). When two galaxies merge, redistribution of stars is inevitable due to potential changes and tidal forces (Peñarrubia et al. 2006).

Since stars are born from gas clouds, processes that relocate gas in the disc also give rise to changes in the stellar radial profile.

Regarding gas rearrangement, gas can be blown out of the disc by stellar feedback from massive stars and then fall back to the disc (Normandeau et al. 1996; Pavel & Clemens 2012; Li et al. 2013). Struck & Elmegreen (2018) showed that such fountains can produce an exponential radial profile. Gas also moves radially into an exponential when it transfers angular momentum due to viscosity proportional to the star formation rate (Lin & Pringle 1987; Wang & Lilly 2022). Furthermore, models show that cosmic gas can flow into the halo of a galaxy and gradually condense onto the galactic disc (Hobbs et al. 2013; Bustard et al. 2016), making changes to the radial distribution of gas. These changes can preserve an initial exponential under reasonable conditions, although the scale length may shrink if the accreted gas has lower specific angular momentum than the disc at the radius where it accretes (Elmegreen et al. 2014).

To build up a connection between an exponential disc and direct radial shifts of stars or indirect shifts via gas rearrangement, Elmegreen & Struck (2016) used a stochastic model which assumes a fixed radial bias in stellar scattering. They showed that scattering with a slight inward bias makes an equilibrium profile that is an exponential divided by radius,  $e^{-r/h}/r$ , which, for galaxies, would be indistinguishable from an exponential beyond one scale length,  $h$ . Inner disk profiles are usually observed to be steeper within the first scale length (Bouquin et al. 2018), which is the inner one-magnitude, but it is difficult to disentangle the possible effects of a disk upturn from a bulge or pseudobulge as the combined colors typically get redder there too (Bakos et al. 2008). This mathematical form is fundamental for a disc geometry, like the Gaussian form is fundamental for one-dimensional scattering in a Galton board. The basic requirement for the exponential is biased scattering toward a reflecting wall; such a wall is automatic in circular coordinates

★ E-mail: jianwu@alumni.iastate.edu (JW), curt@iastate.edu (CS)

because radius cannot be negative. After each particle experiences a sufficient number of scatterings, the exponential scale length derived in the model is  $0.5\lambda/(q-p)$ , where  $\lambda$  is the scattering mean free path, and  $p$  and  $q$  are the outwards and inwards scattering probabilities respectively. Their model requires that  $p+q=1$ , so particles cannot stay still during one scattering time. They also showed that double exponentials with Type II or Type III profiles (see Freeman (1970) and Erwin et al. (2005)) can be generated if the inwards scattering bias assumed in the outer disc is different from the inner disc. Other work that explains the formation of an exponential includes Herpich et al. (2017), Struck & Elmegreen (2019), and Marr (2020), although most of them take a perspective of maximum entropy principle. The maximum entropy approach does not contradict the stochastic scattering model, as the random scattering could be viewed as an instance of how the maximum entropy is realized.

Wu et al. (2022) (hereafter Paper I) studied orbits and angular momentum changes of stars in simulations where exponential discs form due to close star-clump encounters. They found that an inwards scattering bias is not statistically significant in many galactic radii, and suggested that an outwards scattering bias is possible if a clump profile with a shallow density gradient is used in the simulations. Following this suggestion, we want to explore ways to produce an exponential disc in cases where no bias or a slight outwards bias is present during scatterings.

In this paper, we introduce a Markov chain model, simulating stellar scattering in a galactic disc. Basic assumptions and the initial stellar distribution used in the model are presented in Section 2. Stellar profile evolution with different directions of radial scattering bias is given in Section 3. Factors that affect the profile evolution and insights on how to choose model parameters for a specific scattering mechanism are discussed in Section 4. The main results are summarized in Section 5.

## 2 MODEL

The basic model considers an initial disk of stars with a radial profile that deviates significantly from an exponential, such as a flat profile, and evolves it through stellar scattering to a quasi-stationary state. Real galaxies start with more tapered profiles as a result of accretion, mergers, and interactions, and the internal scattering process considered here is likely to adjust this profile by only a small amount. The primary assumption is that the quasi-equilibrium profile for the extreme model is about the same as the quasi-equilibrium profile of a real galaxy, regardless of the different histories.

We use a discrete-time discrete-space Markov chain to study the evolution of the stellar distribution in a galactic disc. We divide the disc into concentric annuli, each with a fixed width of  $d$ . Assuming a maximum disc size  $R$ , the number of annuli in which we count stars is  $N=R/d$ . Let  $n_i(t)$  denote the number of stars in the  $i$ -th annulus at time  $t$ , where  $i=1, 2, 3, \dots, N$ , and  $i=1$  corresponds to the innermost annulus. After each timestep, we assume that a star can stay in its annulus or go to an adjacent one. For a star in the  $i$ -th annulus, where  $i \neq 1$  or  $N$ , the probabilities of moving to the  $(i+1)$ -th annulus and the  $(i-1)$ -th annulus after every timestep are  $p_i$  and  $q_i$ , respectively, and the probability of not moving is  $1-p_i-q_i$ . For a star in the first annulus, it is not allowed to move inward. In this case, the probabilities of moving to the second annulus is  $p_1$ , and the probability of not moving is  $1-p_1$ . This is equivalent to a reflecting inner boundary condition. For a star in the  $N$ -th annulus,

we define the  $(N+1)$ -th "annulus" as the region beyond the radius  $R$  so that the regular transition rule will work here too. Since  $R$  is the maximum radius of the disc, stars in the  $(N+1)$ -th "annulus" are treated as escaping from the galaxy. Therefore, stars in the  $(N+1)$ -th "annulus" stay there forever. Hence the  $(N+1)$ -th "annulus" is an absorbing state.

As real galactic discs may keep growing bigger and do not have a physical edge, the model disc edge  $R$  should be interpreted as a radius beyond which stars are unable to scatter back. The inability to scatter inwards can be caused by processes happening beyond  $R$ , such as the number of scattering centers plummeting at  $R$ . For example, if gas clouds scatter,  $R$  refers to the outer regions that just have smooth gas so they stop scattering. When we say "stars escaping from the galaxy" or "star loss" later in this paper, these stars may still be in the galaxy, but have moved outside of the model disc edge.

Unless otherwise stated, we assume that the probabilities of moving to adjacent annuli are independent of the location of the annulus. Hence we drop the subscript  $i$  in  $p_i$  and  $q_i$ . The evolution of the stellar distribution is described by an  $N+1$  by  $N+1$  transition matrix  $P$  as the following:

$$P = \begin{pmatrix} 1-p & p & 0 & 0 & \dots & 0 & 0 & 0 \\ q & 1-p-q & p & 0 & \dots & 0 & 0 & 0 \\ 0 & q & 1-p-q & p & \dots & 0 & 0 & 0 \\ \cdot & \cdot & \cdot & \cdot & \dots & \cdot & \cdot & \cdot \\ \cdot & \cdot & \cdot & \cdot & \dots & \cdot & \cdot & \cdot \\ \cdot & \cdot & \cdot & \cdot & \dots & \cdot & \cdot & \cdot \\ 0 & 0 & 0 & 0 & \dots & q & 1-p-q & p \\ 0 & 0 & 0 & 0 & \dots & 0 & 0 & 1 \end{pmatrix}, \quad (1)$$

where the  $i, j$  entry is the probability of a star going from the  $i$ -th annulus to the  $j$ -th annulus during one timestep. If  $\pi(t)$  is a row vector representing the numbers of stars in each annulus at time  $t$ , we have

$$\pi(t+1) = \pi(t)P. \quad (2)$$

Here, we made an assumption that  $p, q$ , and the matrix  $P$  do not depend on time  $t$ .

Unless otherwise stated, the disc radius  $R$  and the annulus width  $d$  are chosen as 15 kpc and 1 kpc, respectively. If the radial transition of stars is caused by clumps in the disc, the shift of 1 kpc can be achieved if a star meets a clump of  $10^6 - 10^7 M_\odot$  (Paper I). Thus, based on the N-body results of that paper, we adopt this as the typical scattering length for a massive clump. With  $R=15$  kpc and  $d=1$  kpc, the number of annuli  $N$  is 15. Initially, 100 000 stars are evenly placed in the innermost 10 annuli and the rest of the annuli are empty. Since the initial star number is constant in the inner 10 radial bins, the stellar surface density is proportional to  $1/r$  for  $r \leq 10$  kpc.

Time is measured by the number of timesteps away from the starting time.

To make the Markov chain model generally applicable, we do not tie radial scattering of stars to a certain process at this point. Scattering can be caused by encounters with massive clumps, e.g. resonant scattering at corotation due to spiral arms, or the bar. We will connect stellar scattering to a specific mechanism in Section 4.7 and explain how the model parameters, such as  $p$  and  $q$ , are related to properties of a galaxy.

In a real galaxy, radial scattering of stars is accompanied by angular momentum transport and changes in stellar velocity dispersion. An arbitrary choice of  $p$  and  $q$  can make the total stellar

angular momentum non-conserved. This may not be a serious issue as unbalanced angular momentum can go to gas or dark matter of the galaxy. Changes in velocity dispersion may cause scattered stars and unaffected stars in the same annulus to have different probabilities of getting scattered during next time step. We can partially solve this problem by treating  $p$  and  $q$  as a function of time, as discussed in Section 4.4, while keeping stars undistinguished in an annulus.

### 3 RESULTS

In this section, we show the evolution of the stellar distribution with different choices of the  $(p, q)$  pair in the model. Before that, we present the definition and the property of quasi-stationary distributions.

#### 3.1 The quasi-stationary distribution of the evolution

In our Markov chain model, it is easy to see that all the annular populations, except the  $(N+1)$ -th one, are transient states. According to the properties of Markov chains, the limiting distribution is that all the stars are in the absorbing state. Hence, all the stars move outside of model disc edge. The time to reach this limiting distribution is enormous. Our interest in this model is to study quasi-stationary distributions satisfying the condition that the multi-term ratios  $n_1(t) : n_2(t) : \dots : n_N(t)$  are unchanged with time, although each  $n_i(t)$  decreases with time.

From the definition of the row vector  $\pi(t)$ , we know  $n_1(t), n_2(t), \dots, n_N(t)$  are the first  $N$  entries in  $\pi(t)$ . Using Equation 2, it is easy to obtain the following:

$$\begin{cases} n_1(t+1) - n_1(t) = -pn_1(t) + qn_2(t), \\ n_2(t+1) - n_2(t) = pn_1(t) - (p+q)n_2(t) + qn_3(t), \\ n_3(t+1) - n_3(t) = pn_2(t) - (p+q)n_3(t) + qn_4(t), \\ \dots \\ n_{N-1}(t+1) - n_{N-1}(t) = pn_{N-2}(t) - (p+q)n_{N-1}(t) + qn_N(t), \\ n_N(t+1) - n_N(t) = pn_{N-1}(t) - (p+q)n_N(t). \end{cases} \quad (3)$$

When a quasi-stationary distribution is reached at time  $t$ , we have

$$n_1(t+1) : n_2(t+1) : \dots : n_N(t+1) = n_1(t) : n_2(t) : \dots : n_N(t), \quad (4)$$

which gives the following relation

$$\frac{n_1(t+1) - n_1(t)}{n_1(t)} = \frac{n_2(t+1) - n_2(t)}{n_2(t)} = \dots = \frac{n_N(t+1) - n_N(t)}{n_N(t)}. \quad (5)$$

In this scenario, we let  $\beta(t)$  denote the fractions in Equation 5, i.e.

$$\beta(t) := \frac{n_1(t+1) - n_1(t)}{n_1(t)}. \quad (6)$$

Adding up all the numerators and all the denominators, Equation 5 gives

$$\beta(t) = \frac{\sum_{i=1}^N n_i(t+1) - \sum_{i=1}^N n_i(t)}{\sum_{i=1}^N n_i(t)}. \quad (7)$$

This means that  $\beta(t)$  is not only the relative change of the star number in each annulus, but also the relative change of total stars in the disc. Replacing numerators in Equation 5 with the right sides

of Equation 3, we obtain analytic equations that a quasi-stationary distribution satisfies:

$$\begin{aligned} \frac{-pn_1(t) + qn_2(t)}{n_1(t)} &= \frac{pn_1(t) - (p+q)n_2(t) + qn_3(t)}{n_2(t)} \\ &= \frac{pn_2(t) - (p+q)n_3(t) + qn_4(t)}{n_3(t)} \\ &\dots \\ &= \frac{pn_{N-2}(t) - (p+q)n_{N-1}(t) + qn_N(t)}{n_{N-1}(t)} \\ &= \frac{pn_{N-1}(t) - (p+q)n_N(t)}{n_N(t)}. \end{aligned} \quad (8)$$

To simplify Equation 8,  $n_i(t)/n_{i+1}(t)$  is denoted by  $f_i$ , where  $i = 1, 2, 3, \dots, N-1$ . Adding  $(p+q)$  to each fraction in Equation 8 and then dividing it by  $q$ , the equation becomes

$$\begin{aligned} 1 + \frac{1}{f_1} &= \frac{p}{q}f_1 + \frac{1}{f_2} \\ &= \frac{p}{q}f_2 + \frac{1}{f_3} \\ &\dots \\ &= \frac{p}{q}f_{N-2} + \frac{1}{f_{N-1}} \\ &= \frac{p}{q}f_{N-1}. \end{aligned} \quad (9)$$

The equation above is a set of  $N-1$  equations. When  $p/q$  is given, the  $f_i$  are  $N-1$  unknowns and can be solved for. After obtaining  $f_i$ , we can easily construct a quasi-stationary distribution. From this analysis, we see that the quasi-stationary distribution of the evolution is determined uniquely by the  $p/q$  ratio, regardless of the initial distribution of stars.

When a quasi-stationary distribution is reached, the relative change of the star number during one timestep can be written as

$$\beta(t) = \frac{-pn_1(t) + qn_2(t)}{n_1(t)} = -p + \frac{q}{f_1}. \quad (10)$$

In this limit  $f_1$ , and thus,  $\beta(t)$  become time independent. Thenceforth, the number of stars decays exponentially with time at each radius.

#### 3.2 Example stellar profile evolutions

##### 3.2.1 Stellar profile evolution when $p = q = 0.1$

Figure 1 shows the number of stars and the surface density of the number in each annulus from  $t = 0$  to  $t = 120$ . Due to the scattering of stars to adjacent annuli, annuli beyond 10 kpc gradually get filled with stars and annuli within 10 kpc lose stars. As the number of stars changes in each radial bin, the surface density profile evolves with time. On the right panel, one can see that the rate of the profile change slows down as the difference between two neighbouring curves narrows. At  $t = 120$ , the surface density looks like an exponential with a cusp at the central plus a dip near the edge.

Figure 2 shows the profile evolution in a longer term from  $t = 120$  to  $t = 2400$ . Both panels show that the number of stars in every radial bin decreases with time. On the right panel, the shape of the curves hardly changes, indicating that the ratio  $n_1(t) : n_2(t) : \dots : n_{15}(t)$  has converged. This means the profile has reached a quasi-stationary state at  $t = 2400$ . From the right panel, one can also see that the distance between two neighbouring curves is almost

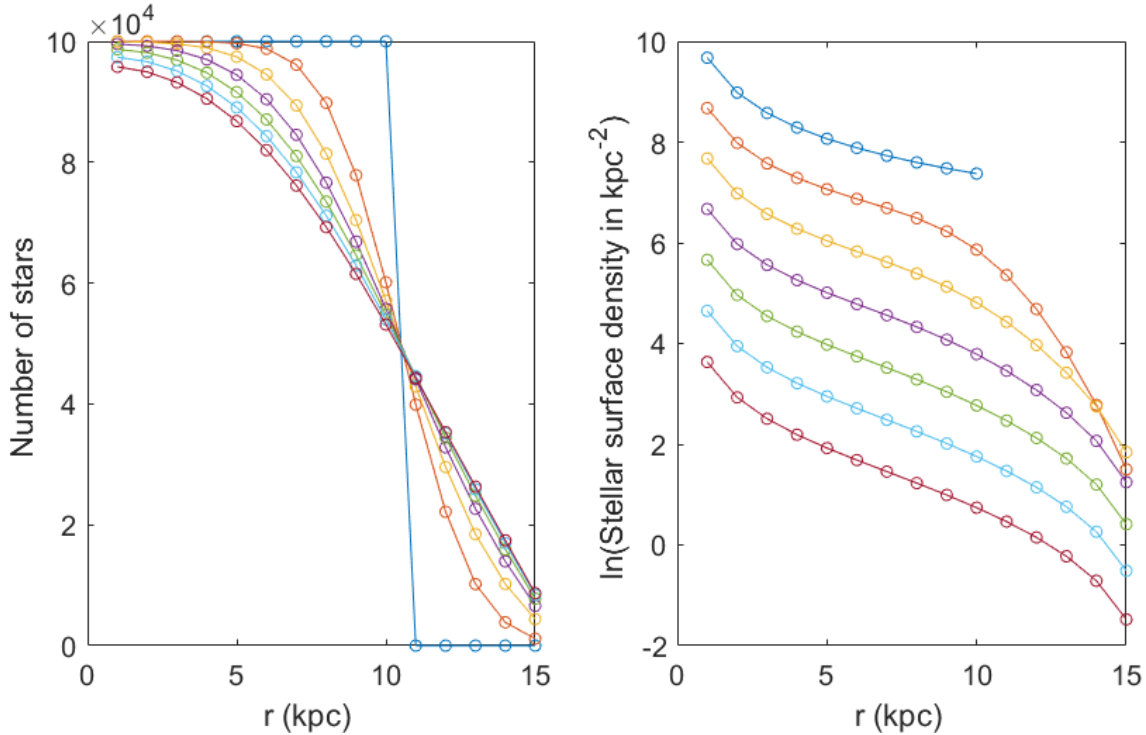


**Figure 1.** Time evolution of the stellar distribution from  $t = 0$  to  $t = 120$  when  $p = q = 0.1$ . The left panel shows the number of stars in each annulus and the right panel shows the surface density, i.e. the number of stars divided by the area of each annulus. On both panels, the curves from top to bottom corresponds to  $t = 0$  (blue), 20 (orange), 40 (yellow), 60 (purple), 80 (green), 100 (light blue), and 120 (dark red) respectively. On the right panel, curves, except the blue one, are shifted downwards by one unit successively to give a clear view.

constant after  $t = 400$ . Since the y-axis is in a logarithm scale, this reveals that the number of stars at each radius decays exponentially with time, as predicted by Equation 10 in the quasi-static limit.

To better understand how fast the profile converges to the quasi-stationary distribution, we use  $n_1(t)/n_{15}(t)$  as an indicator. The blue solid curve on Figure 3 shows  $\ln(n_1(t)/n_{15}(t))$  as a function of time for  $p = q = 0.1$ . The  $n_1(t)/n_{15}(t)$  ratio decreases rapidly before  $t = 120$ , but the decline is hardly noticeable afterwards. This agrees with the profile change rate reflected by Figure 1 and 2. As the profile approaches the quasi-stationary distribution, the  $n_1(t)/n_{15}(t)$  ratio converges to a constant. The values of the ratio are 11.05, 9.90, and 9.87, at  $t = 120$ , 500, and 1000, respectively. Beyond  $t = 1000$ , the value change is less than 0.01.

Figure 4 shows the total number of stars in the galactic disc from  $t = 0$  to  $t = 2400$ . As we mentioned before, the star loss is due to the outwards scattering at 15 kpc. When time is greater than 100, the curve confirms a clear exponential decay of stars. After the quasi-stationary state is reached, the relative change per timestep  $\beta(t)$  is -0.0010. This value is small because only the scattering of the outermost annulus contributes to it and stars in that annulus are only 1% of the total disc stars. Please note that the star loss in a short term is not significant. From  $t = 0$  to  $t = 120$ , the disc loses 6.47% of initial stars.

When using the model to explain the formation of an exponential disc, we can stop the model at  $t = 120$  to avoid excess star losses. A key point revealed by the model is that the scattering of stars into adjacent annuli can lead to rapid profile changes towards a near-exponential with the cost of losing a few percent of the total stars. In a real galaxy, many processes can be responsible for the

scattering of stars. If the process has a short lifetime, the star loss at the model disc edge will stop as the process ends, so the disc will not experience the long-term star loss. If the scattering process does have a long lifetime, such as scattering by spiral arms at corotation, then the long-term star loss rate may be exceeded by input processes, such as star formation fed by gas accretion. The losses would not be an issue in such cases either. We run our models for a long time in order to show detailed properties of quasi-stationary distribution rather than to present star losses.

The curves in Figure 2 can be viewed as numerical solutions to Equation 8 or Equation 9. In Equation 9, the expressions on each side of the equal signs all have the same form, except the first one and the last one. If the two boundary expressions got removed, a trivial solution would be that all the  $f_i$  share the same value. Since  $f_i$  is the star number ratio between neighbouring annuli, this means that the star number would decay exponentially with radius and the star surface density would have the form of  $e^{-r/h}/r$ . When taking the boundary expressions into account, specific restrictions are directly applied to annuli close to 1 kpc or 15 kpc. Annuli in the middle, however, are less affected. From 5 to 10 kpc, the star surface density should be approximately  $e^{-r/h}/r$ . As  $1/r$  changes much more slowly than  $e^{-r/h}$ , the  $e^{-r/h}/r$  profile looks very similar to  $e^{-r/h}$  in this radius range. When looking at the right panel of Figure 2, one can see that the surface density in this range is indeed close to a straight line, indicating a profile of  $e^{-r/h}$ .

Now let's examine annuli near 1 kpc. Plugging the values of  $p$  and  $q$  into Equation 10, the equation can be written as

$$\frac{\beta(t)}{0.1} = \frac{-n_1(t) + n_2(t)}{n_1(t)}. \quad (11)$$

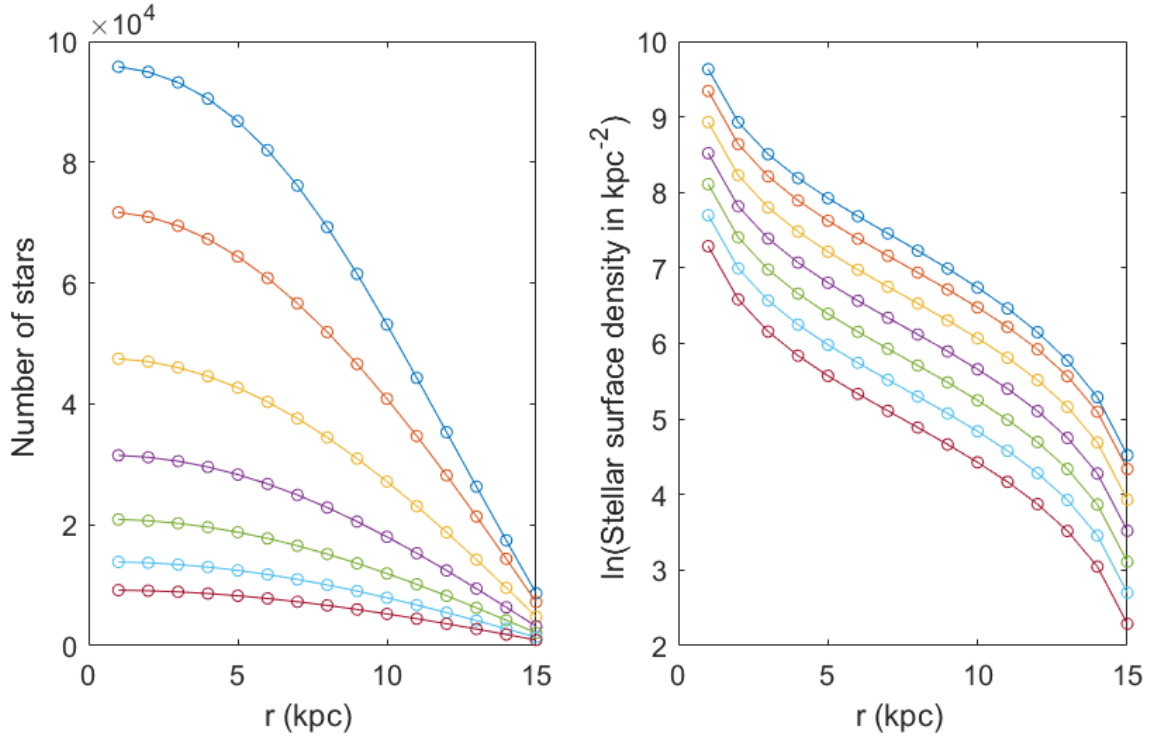


**Figure 2.** Stellar profile evolution continued from Figure 1. On both panels, the curves from top to bottom corresponds to  $t = 120$  (blue), 400 (orange), 800 (yellow), 1200 (purple), 1600 (green), 2000 (light blue), and 2400 (dark red) respectively. Curves on the right are not shifted downwards artificially. The downwards motion is caused by star loss at the edge of the disc.

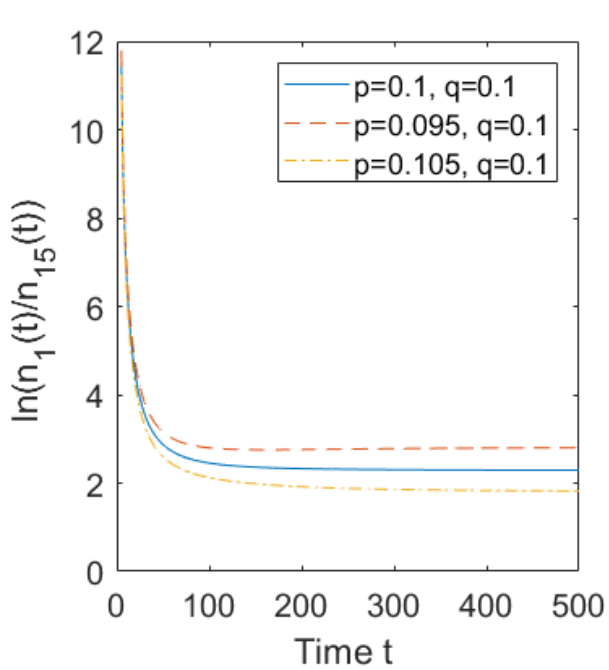


**Figure 3.** Time evolution of the star number ratio of the first annulus to the fifteenth annulus. The model starts from an  $1/r$  disc with an initial size of 10 kpc. The blue solid curve, the orange dashed curve, and the yellow dash dotted curve represent different choices of  $p, q$ .

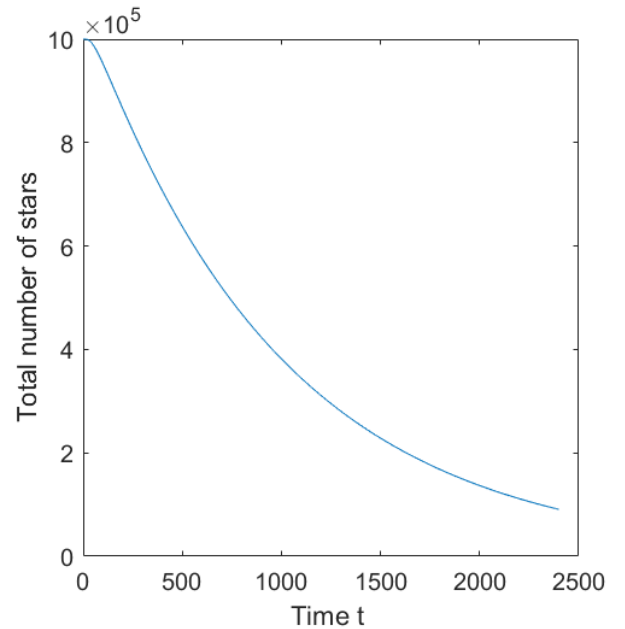


**Figure 4.** Time evolution of the total number of stars within 15 kpc when  $p = q = 0.1$ . The model starts from an  $1/r$  disc with an initial size of 10 kpc.

Since  $|\beta(t)|$  is much less than 0.1, the relative change from  $n_1(t)$  to  $n_2(t)$  is small, so  $f_1$  is close to 1. Using Equation 9, we know that an  $f_1$  value around 1 makes  $f_2$  close to 1 as well. It is easy to see



from here that the star numbers in annuli near 1 kpc are about the same, which gives a surface density profile of  $1/r$ . This corresponds to the central cusps on the right panel of Figure 2. In a real galaxy, the predicted overdensity at the center is usually treated as a bulge with a distinct origin, whereas it could be the remnant of scattering in the disc.

As for annuli near 15 kpc, the last two lines in Equation 9 indicate that  $f_{N-1}$  is greater than  $f_{N-2}$ . If taking this as a condition to study the relation between  $f_{N-2}$  and  $f_{N-3}$ , one can obtain that  $f_{N-2}$  is greater than  $f_{N-3}$ . Therefore, the radial decay of the star number accelerates near the model disc edge, showing as the dip at 15 kpc on the right panel of Figure 2. When combining the profile here with the part from 5 to 10 kpc, it resembles a Type II exponential (see Freeman (1970)). The quasi-stationary distribution near the model disc edge is sensitive to the scattering in the  $N$ -th annulus. If the star loss rule is modified in the model, the profile near the edge will change. For real galaxies, stars in the outer part will continue to scatter as long as there are scattering perturbations such as gas clumps; there may not be an absorbing boundary. Determining the model disc edge and measuring the surface density there are usually hard owing to low brightness.

### 3.2.2 Stellar profile evolution when $p = 0.095$ and $q = 0.1$

Figures 5 and 6 show the stellar profile changes when  $p=0.095$  and  $q=0.1$ . Figure 5 illustrates a short-term evolution from  $t = 0$  to  $t = 120$ , and Figure 6 illustrates a long-term evolution  $t = 120$  to  $t = 2400$ . Curves, except for  $t = 0$ , on the right panel of Figure 5 are shifted downwards by one unit successively to give a clear view. From the two figures, one can see that the rate of the profile evolution slows down with time and that the profile changes beyond  $t = 120$  are small. At  $t = 2400$ , the stellar number distribution has reached a quasi-stationary state, and the corresponding surface density distribution is a near-exponential with a shape similar to the case of  $p = q = 0.1$ . From Figure 6, one can also see the decay of the star number with time in every annulus due to the outwards scattering at 15 kpc. At the quasi-stationary state, the relative star change per timestep  $\beta(t)$  is  $-0.00071$ . Its magnitude is less than that for  $p = q = 0.1$ . The total star loss in the short-term from  $t = 0$  to  $t = 120$  is 5.08%, also less than that for  $p = q = 0.1$ . These results make sense because the outward scattering at 15 kpc becomes weaker as  $p$  goes from 0.1 to 0.095.

When comparing the left panel of Figure 5 to that of Figure 1, a noticeable difference is that annuli near 1 kpc in Figure 5 gain stars while those in Figure 1 do not. The gain is caused by the inwards scattering bias due to  $p < q$ . The bias also leads to a steeper stellar gradient near 1 kpc for the quasi-stationary state. At the quasi-stationary state, Equation 10 gives

$$f_1 = \frac{q}{\beta(t) + p}. \quad (12)$$

Since  $|\beta(t)|$  is very small compared to  $p$ ,  $f_1$  is close to  $q/p = 1.053$  when  $p = 0.095$  and  $q = 0.1$ . This means that star numbers in the second annulus are about 5% less than those in the first annulus. Using the first line of Equation 9, it is easy to see that  $f_1$  is close to  $f_2$  when we approximate the  $f_1$  on the right side using  $q/p$ . Hence, a value of  $f_1$  greater than 1 makes  $f_2$  greater than 1 as well, so the number of stars in the third annulus is less than that in the second annulus. When comparing the left panel of Figure 6 to that of Figure 2, one can see that star numbers near 1 kpc decline clearly with  $r$  for  $p = 0.095$  and  $q = 0.1$ , but vary much less for  $p = q = 0.1$ .

The red dashed line in Figure 3 shows the time evolution of  $\ln(n_1(t)/n_{15}(t))$  for  $p=0.095$  and  $q=0.1$ . Similar to the case of  $p = q = 0.1$ , the  $n_1(t)/n_{15}(t)$  ratio changes quickly before  $t = 120$ , confirming the relatively fast profile change in the short-term. When the quasi-stationary state is reached, the ratio converges to 16.51, which is greater than that of  $p = q = 0.1$ . This larger ratio is not only due to the steeper gradient in the first few annuli, as explained in the previous paragraph, but also owing to the sharper star number decrease in the middle annuli. On the right panel of Figure 6, the linear fit of the quasi-stationary surface density from 6 kpc to 10 kpc gives a exponential profile with a scale length of 3.81 kpc. The fitting in the same radial interval on the right panel of Figure 2 gives a scale length of 4.41 kpc. Hence, the case of  $p=0.095$  and  $q=0.1$  has a steeper gradient than  $p = q = 0.1$  in the middle annuli, in addition to the annuli near 1 kpc. We will discuss the relation between  $p/q$  and the scale length later in this paper.

### 3.2.3 Stellar profile evolution when $p = 0.105$ and $q = 0.1$

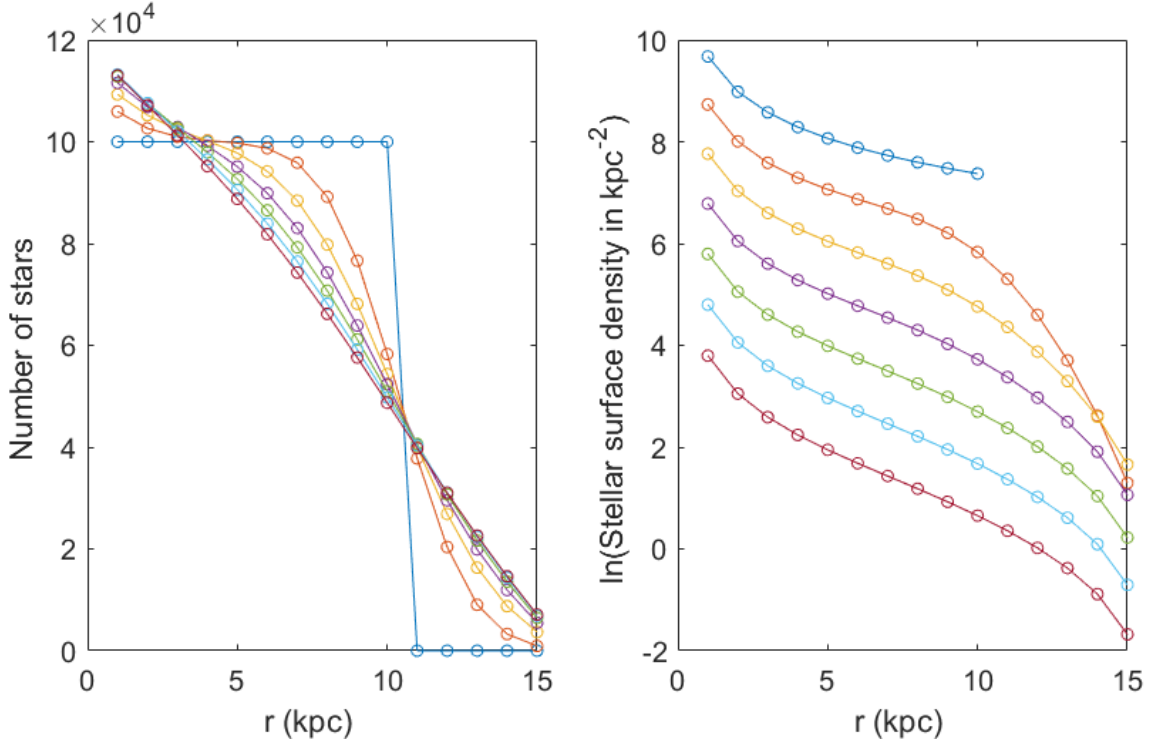
After presenting the  $p = q$  case and the  $p < q$  case, we now illustrate a  $p > q$  case. When comparing it to the  $p = q$  case, many results are the opposite of the comparison between  $p < q$  and  $p = q$ .

Figure 7 and 8 show the profile changes for  $p = 0.105$  and  $q = 0.1$  from  $t = 0$  to  $t = 120$  and  $t = 120$  to  $t = 2400$ , respectively. As before, the rate of profile changes declines with time, and the disc converges to a quasi-stationary distribution with a near-exponential profile. Since the outwards scattering at 15 kpc is stronger than the previous two cases, the star loss in the case is the largest among the three scenarios. From  $t = 0$  to  $t = 120$ , the disc loses 8.08% of the total star. At the quasi-stationary state, the relative change of the star number during a timestep is  $\beta(t) = -0.0014$ .

For  $p = 0.105$ ,  $q = 0.1$ , and  $\beta(t) = -0.0014$ , Equation 12 gives a  $f_1$  value of 0.965. As shown in the previous subsection,  $f_1$  is close to  $f_2$  at the quasi-stationary state, so  $f_2$  is also less than 1. Therefore, the star numbers in the first few annuli increase with radius as shown on the left panel of Figure 8. This also means that the surface density profile near 1 kpc declines more slowly than the  $p = 0.1$  case and the  $p = 0.095$  case.

The yellow dash dotted curve in Figure 3 shows the change of  $n_1(t)/n_{15}(t)$  with time for  $p = 0.105$ . As before, fast changes occur before  $t = 120$ . The  $n_1(t)/n_{15}(t)$  ratio converges to 6.1313, less than that of  $p = 0.1$ . The linear fit of the quasi-stationary surface density from 6 to 10 kpc on the right panel of Figure 8 gives a scale length of 5.17 kpc, corresponding to a shallower gradient than  $p = 0.1$ .

In summary, any of the three  $(p, q)$  pairs shown in this section, regardless the direction of the radial scattering bias, is able to generate a stellar profile almost identical to the quasi-stationary profile within 120 time steps. During this time period, the star loss at the model disc edge is less than 10% for all the three cases. The near-exponential shape of the surface density profile appears within 40 time steps. As the model only requires stellar scattering in each annulus, these results indicate that many mechanisms that spread stars along the radial direction have the potential to contribute to the formation of an exponential disc. The actual time length of 40 steps depends on the efficiency of the stellar scattering mechanism, i.e. how long it takes the process to scatter 10% of stars into adjacent annuli. If the stellar scattering is due to giant clouds, Paper I indicates that 40 steps can be about 8 Gyr. If the initial stellar number distribution is centrally concentrated instead of being uniform, the time it takes to reach a near-exponential profile should be significantly less.



**Figure 5.** Time evolution of the stellar distribution from  $t = 0$  to  $t = 120$  when  $p = 0.095$  and  $q = 0.1$ . Colors of the curves represent different time in the same way as Figure 1. On the right panel, curves, except the blue one, are shifted downwards by one unit successively to give a clear view.

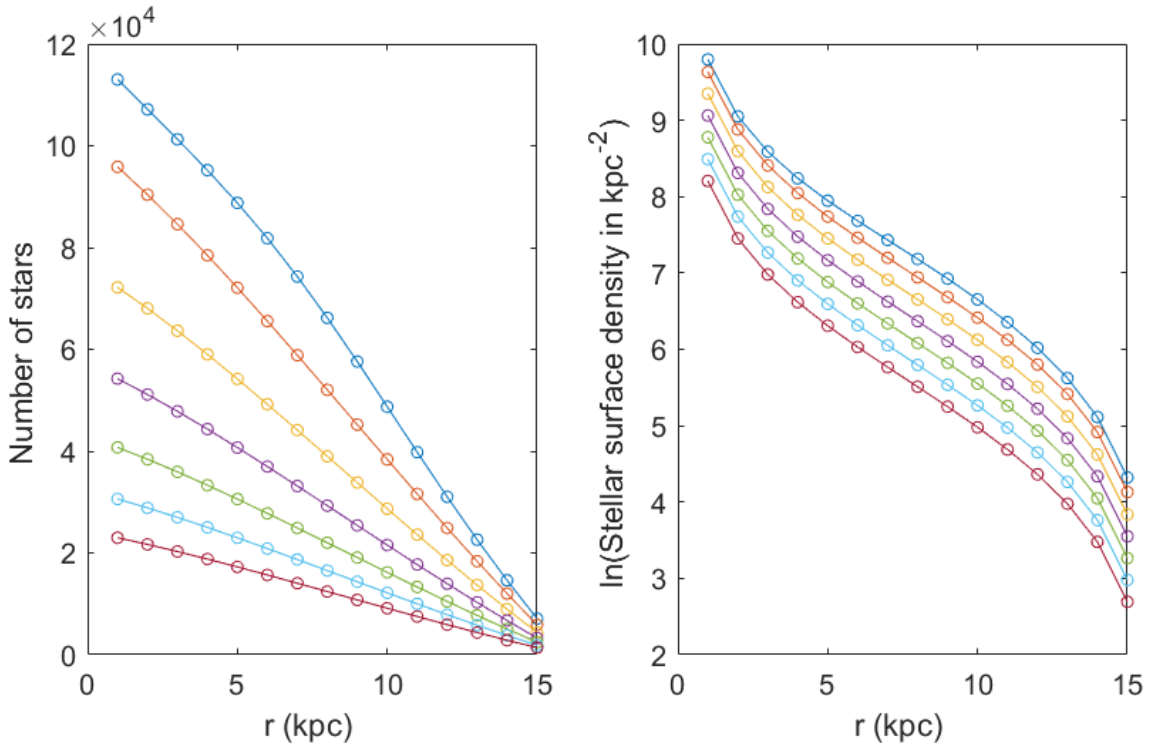


**Figure 6.** Stellar profile evolution from  $t = 120$  to  $t = 2400$  when  $p = 0.095$  and  $q = 0.1$ . It is a continuation of Figure 5. Colors of the curves represent different time in the same way as Figure 2. Curves on the right are not shifted downwards artificially. The downwards motion is caused by star loss at the edge of the disc.

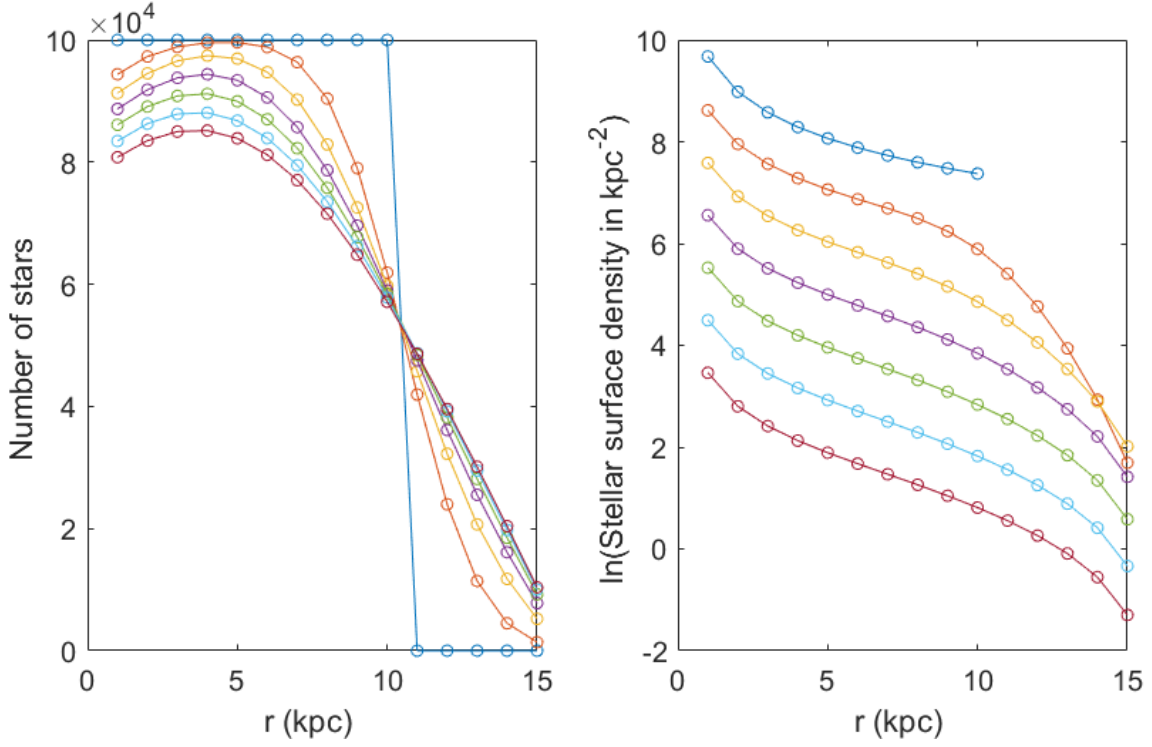


**Figure 7.** Time evolution of the stellar distribution from  $t = 0$  to  $t = 120$  when  $p = 0.105$  and  $q = 0.1$ . Colors of the curves represent different time in the same way as Figure 1. On the right panel, curves, except the blue one, are shifted downwards by one unit successively to give a clear view.

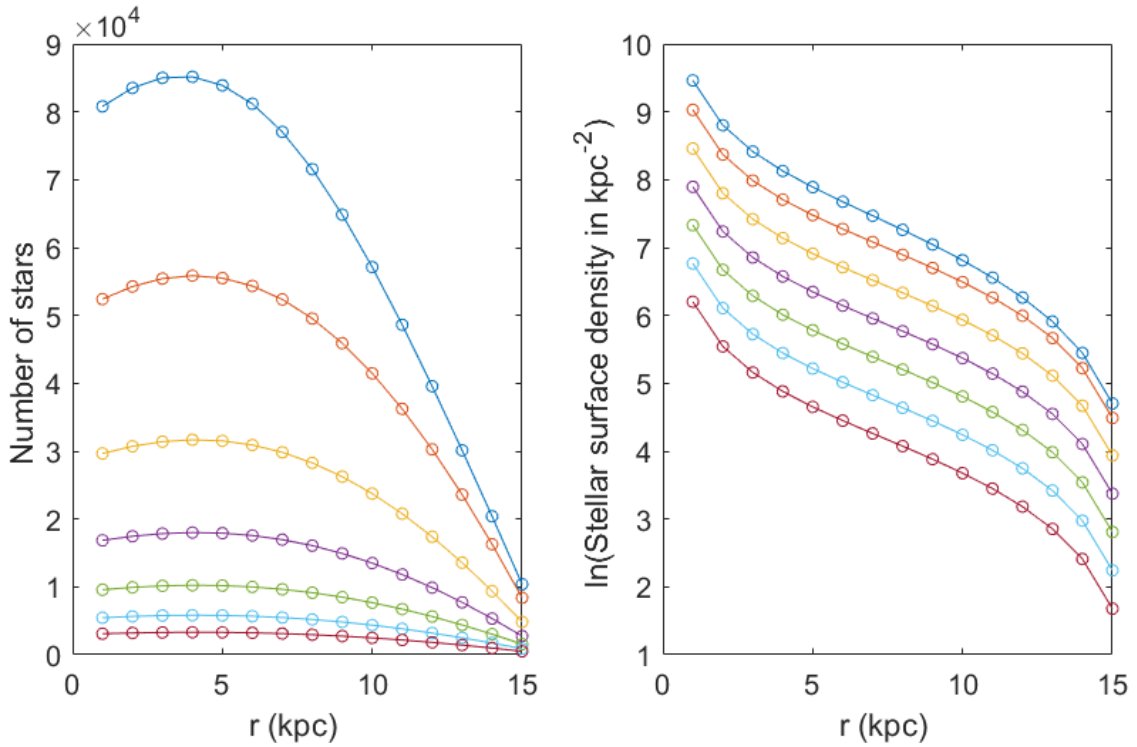


**Figure 8.** Stellar profile evolution from  $t = 120$  to  $t = 2400$  when  $p = 0.105$  and  $q = 0.1$ . It is a continuation of Figure 7. Colors of the curves represent different time in the same way as Figure 2. Curves on the right are not shifted downwards artificially. The downwards motion is caused by star loss at the edge of the disc.



### 3.3 Effects from initial stellar distribution

In Section 3.1, we showed that the quasi-stationary distribution that the model converges to is independent of the initial profile of stars. Nevertheless, the initial distribution has an impact on the time needed to reach the quasi-stationary state. Results from the previous subsection showed the profile evolution starting from a  $1/r$  disc. In this subsection, we present profile changes with other initial profiles.

Figure 9 shows profile changes starting from a Sérsic profile with the Sérsic index  $n$  of 0.5 combined with a drop in stellar surface density at 14 kpc. To be more specific, the initial Sérsic profile satisfies  $\Sigma(r) \propto e^{-r^2/h^2}$ , with a scale length  $h$  of 5.4 kpc. The drop indicates a ring-shaped pattern in the light distribution at 14 kpc. The scattering probabilities used in the model are  $p = q = 0.1$ . Curves in the figure reflect profiles from  $t = 0$  to  $t = 120$ . In Figure 9, the stellar profile evolves towards an near-exponential as expected. At  $t = 120$ , the  $n_1(t)/n_{15}(t)$  ratio is 18.56, greater than 11.05, which is the ratio at the same time in the case of  $1/r$  disc. As the quasi-stationary ratio is 9.87, the evolution stage reached at  $t = 120$  in this trial is behind that in the  $1/r$  trial. The total star loss from  $t = 0$  to  $t = 120$  is 3.86 %.

Figure 10 shows disc evolution starting from another Sérsic profile superposed with a few fluctuations in stellar surface density. The Sérsic density distribution satisfies  $\Sigma(r) \propto e^{-\sqrt{r}/h}$ , with  $h = 0.14$  kpc. Hence, the Sérsic index  $n$  is 2. In the trial, we continue to use  $p = q = 0.1$ . Curves in the figure show profile changes from  $t = 0$  to  $t = 240$ . On the right panel of Figure 10, one can see that the fluctuations in stellar surface density quickly get smoothed out and that the magnitude of the slope from 5 to 10 kpc gradually declines with time, indicating an increasing scale length. The  $n_1(t)/n_{15}(t)$  ratios at  $t = 120$  and  $t = 240$  are 51.53 and 16.28, respectively. Therefore, the evolution stage reached at  $t = 240$  is still behind the  $t = 120$  stage in the  $1/r$  trial. The star loss from  $t = 0$  to  $t = 240$  is 7.40 %, which is greater than the total star loss at  $t = 120$  in the  $1/r$  trial. It is clear that this run will suffer more star loss than the  $1/r$  trial when they reach the same evolution stage. This indicates that the initial stellar distribution affects the amount of star loss.

Figure 11 shows  $\ln(n_1(t)/n_{15}(t))$  as a function of time for the two runs presented in Figure 9 and 10. The curve for the  $1/r$  run is also added to make the comparison easier. In the figure,  $n_1(t)/n_{15}(t)$  for the three runs converges to the same value, confirming that they share the same quasi-stationary state. Regarding the time it takes to reach the quasi-stationary state, the  $1/r$  run is the shortest and the Sérsic run with  $n = 2$  is the longest. When looking at the  $t = 0$  curve on the left panel of Figure 1, 9, and 10, one can see that an initial distribution close to the quasi-stationary distribution, i.e. the  $1/r$  disc, uses a short time to converge and an initial distribution far from it, i.e. the Sérsic profile with  $n = 2$ , takes a long time to reach it. Even if the two Sérsic runs take a longer time to reach the quasi-stationary states, the profiles start to look like a near-exponential within 40 time steps, which is comparable to the  $1/r$  run.

## 4 DISCUSSION

### 4.1 Profile change rate

As mentioned in Section 3.1, the quasi-stationary distribution depends on the ratio of  $p/q$ . Given a fixed  $p/q$ , the magnitude of  $p$  or  $q$  determines the profile change rate. Roughly speaking, the profile change rate is linearly correlated with the magnitude of  $p$  or  $q$ , when  $p$  and  $q$  are small. The star number changes during one time step

in case of  $p = q = 0.1$  are similar to the changes during two time steps in case of  $p = q = 0.05$ .

Figure 12 shows the time evolution of  $\ln(n_1(t)/n_{15}(t))$  for three runs using the same  $p/q$  ratio but different  $p$  values. The initial stellar profile for all three runs is the  $1/r$  disc. To better see the linear relation between the profile change rate and the magnitude of  $p$  or  $q$ ,  $\ln[(p+q)t]$  is plotted on the horizontal axis, instead of  $t$ . From the figure, one can see that  $n_1(t)/n_{15}(t)$  of all the runs quickly converges to the same curve. This means that if using a certain value of  $n_1(t)/n_{15}(t)$  as a milestone of the profile evolution, the time steps needed to reach the milestone in the runs are inversely proportional to  $p+q$ . In other words, the profile change rates are proportional to  $p+q$ .

The total star losses from the beginning to  $\ln(n_1(t)/n_{15}(t)) = 2.40$  for  $p = 0.1$ ,  $p = 0.05$ , and  $p = 0.025$  in Figure 12 are 6.47%, 6.56%, and 6.58%, respectively. It seems that the star loss between two evolution stages is not sensitive to  $p+q$ , or the profile change rate.

### 4.2 Stellar profile at the disc center

In Section 3, we showed that the stellar surface density profile of a quasi-stationary state has an upturn down to the center. In this subsection, we briefly discuss the shape of the upturn and its dependence on  $p/q$ .

For simplicity, we fit the surface density  $\Sigma(r)$  at low  $r$  with a power law equation, i.e.

$$\Sigma(r) \propto r^\nu. \quad (13)$$

As the shape of the quasi-stationary distribution depends on  $p/q$ , the best fitting exponent  $\nu$  is a function of  $p/q$ . The black dashed curve in Figure 13 shows the fitting result by using the surface density profile at  $r < 3$  kpc. As  $p/q$  increases,  $\nu$  becomes less negative. When  $p/q = 1$ ,  $\nu$  is about -1. This is consistent with our analysis in Section 3.2.1.

We can also use Equation 12 to estimate  $\nu$ . Because  $|\beta(t)|$  is very small,  $f_1$  is close to  $q/p$ . Using the definition of  $f_1$ , we obtain  $n_1/n_2 \approx q/p$ . As  $r\Sigma(r)$  is proportional to the number of stars in the annulus at radius  $r$ , the ratio of  $n_1/n_2$  can be written as

$$\frac{n_1}{n_2} = \frac{\Sigma(1)}{2\Sigma(2)}. \quad (14)$$

Using Equation 13,  $\Sigma(1)/\Sigma(2)$  is equal to  $0.5^\nu$ . As  $n_1/n_2 \approx q/p$ , Equation 14 becomes  $q/p \approx 0.5^\nu/2$ , which can be rewritten as

$$\nu \approx \frac{-\ln(p/q)}{\ln(0.5)} - 1. \quad (15)$$

The red solid curve in Figure 13 shows the value of  $\nu$  by using Equation 15. It matches up with the black curve when taking uncertainty into consideration.

### 4.3 Disc scale length

In Section 3, we showed the quasi-stationary distributions for  $p/q = 0.95, 1, \text{ and } 1.05$ . The exponential scale lengths of these distributions measured from 6 kpc to 10 kpc are 3.81 kpc, 4.41 kpc, and 5.17 kpc respectively. In this subsection, we look at the scale length in a wider range of  $p/q$ , and study other factors in the model that can influence the scale length.

The solid blue in Figure 14 shows the scale length of the quasi-stationary state from 6 kpc to 10 kpc as a function of  $p/q$ , given that other parameters in the model are chosen according to

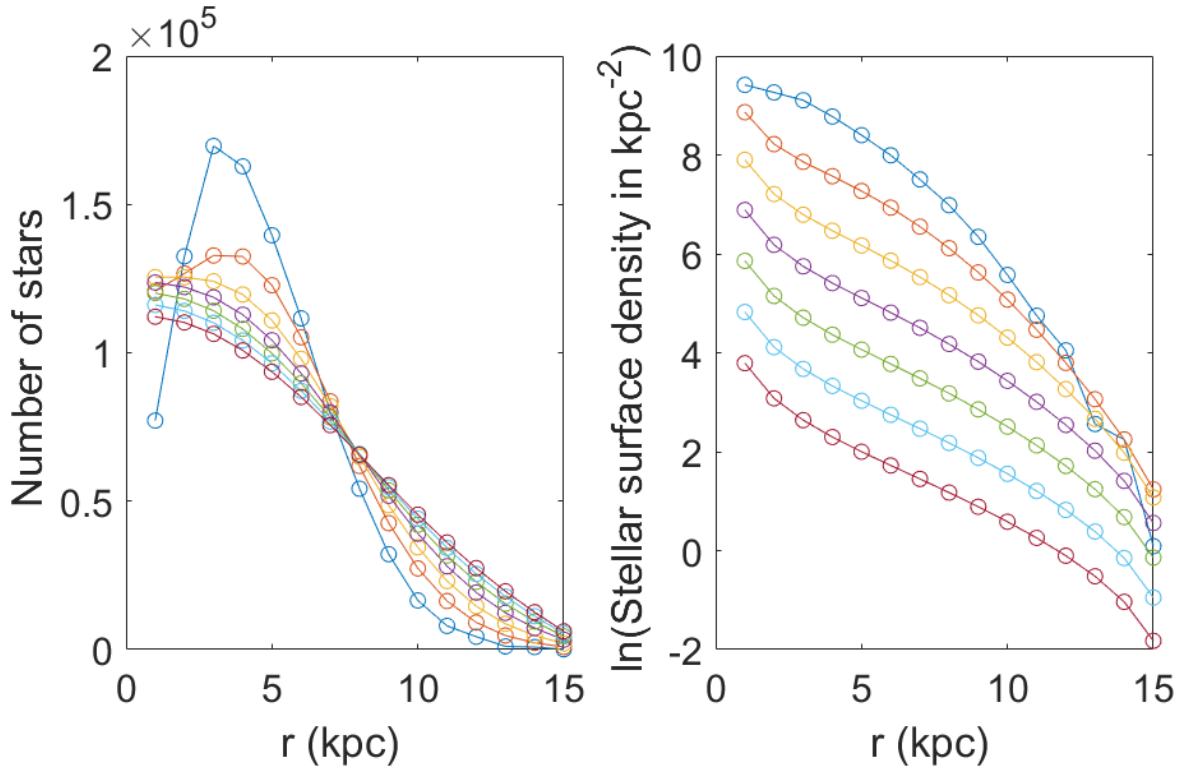


**Figure 9.** Stellar profile evolution of an initial Sérsic disc with the index  $n$  of 0.5 from  $t = 0$  to  $t = 120$  when  $p = 0.1$  and  $q = 0.1$ . A drop in stellar surface density at 14 kpc, indicating a ring-shaped pattern in the light distribution, is superposed on the initial profile. Colors of the curves represent different time in the same way as Figure 1. On the right panel, curves, except the blue one, are shifted downwards by one unit successively to give a clear view.

the description in Section 2. As  $p/q$  increases from 0.5 to 1.4, the scale length goes up with a growing rate, indicating that the surface density profile has a much shallower decline. When  $p/q$  goes beyond 1.44, the slope of the quasi-stationary surface density from 6 kpc to 10 kpc becomes positive, leading to a density profile increasing with the galactic radius. In contrast, when  $p/q$  is much smaller than 1, the surface density gradient from 6 kpc to 10 kpc is close to the gradient near 1 kpc and 15 kpc, making the cusp at 1 kpc and the dip at 15 kpc hard to notice. For example, Figure 15 shows the quasi-stationary surface density for  $p/q = 0.5$ . The overall profile resembles a straight line.

To illustrate the connection between  $p/q$  and the scale length  $h$ , Equation 12 is a good starting point.  $f_1$ , the ratio of stars in the first annulus to those in the second, will go down as  $p/q$  increases, given that  $|\beta(t)|$  in general is small. Ratios between other adjacent annuli behave in a similar way as all the  $f_i$  are related by Equation 9. Informally speaking, when the ratios decrease towards 1, the quasi-stationary surface profile becomes flatter. Thus the disk scale length  $h$  rises. By the way, when  $p/q$  is greater than 1.2, the outwards scattering bias can cause a significant star loss before the profile converges to the quasi-stationary state. When the model starts with the  $1/r$  disc,  $p/q = 1.2$  results in a star loss of about 45%. On the contrary, a  $p/q$  much smaller than 1 gives a star loss less than 4%.

The disc scale length of the quasi-stationary state depends on the annulus width  $d$ . The blue curve in Figure 14 uses a Markov chain model with a disc radius  $R$  of 15 kpc and an annulus width  $d$  of 1 kpc. If keeping  $R$  unchanged but modifying  $d$  to 0.5 kpc, the number of annuli  $N$  changes from 15 to 30. In this scenario, the quasi-stationary state for a given  $p/q$  is different, and the relation

between the scale length  $h$  and the  $p/q$  ratio is illustrated by the dashed orange curve in Figure 14. As  $p/q$  increases, the curve surges as the  $d = 1$  kpc case but with a faster rate. The scale length for  $d = 0.5$  kpc is less than  $d = 1$  kpc when  $p/q < 1$ , but surpasses  $d = 1$  kpc when  $p/q > 1$ .

To understand the difference between the two curves, one can consider the star numbers at two galactic radii, e.g., 7 kpc and 8 kpc. When  $d = 1$  kpc, these two radii correspond to two neighbouring annuli. In contrast, when  $d = 0.5$  kpc, an additional annulus at 7.5 kpc is placed between 7 kpc and 8 kpc. In this case, the star number balance between 7 kpc and 8 kpc is maintained through the additional annulus. The star number ratio between 7 kpc and 8 kpc is a product of the 7 kpc to 7.5 kpc ratio and the 7.5 kpc to 8 kpc ratio. When a radial scattering bias exists in the disc, this additional annulus enlarges the star number gap between 7 kpc and 8 kpc in the quasi-stationary distribution, as if the scattering bias doubles. In Figure 14, the scale length for  $d = 0.5$  kpc models when  $p/q = 0.9$  is 2.55 kpc, similar to the value of  $h = 2.54$  kpc for  $d = 1$  kpc models when  $p/q = 0.8$ . Likewise, the scale length for  $d = 0.5$  kpc when  $p/q = 1.1$  is 9.11 kpc, similar to the value of  $h = 9.28$  kpc for  $d = 1$  kpc when  $p/q = 1.2$ . One can see that the scale length for  $d = 0.5$  kpc at a given  $p/q$  is close to that for  $d = 1$  kpc at a  $p/q$  value about two times farther away from  $p/q = 1.0$ .

As mentioned in the introduction, Elmegreen & Struck (2016) studied the dependence of the scale length on the scattering probabilities given an inwards bias. The scale length  $0.5\lambda/(q-p)$  given in their model increases at a growing rate as the inwards scattering bias gets weaker, i.e. as  $q$  becomes slightly greater than  $p$ . This qualitatively agrees with our Figure 14, regardless of what  $d$  is cho-

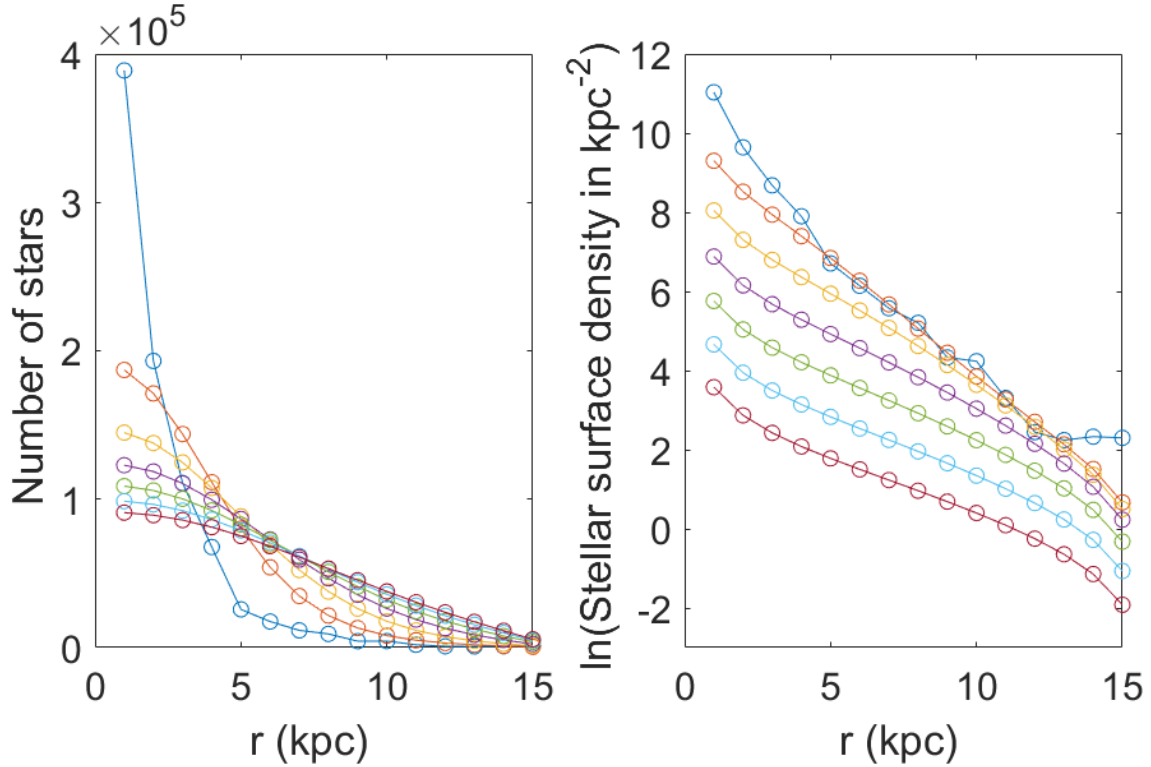


**Figure 10.** Stellar profile evolution of a Sérsic disc with the index  $n$  of 2 from  $t = 0$  to  $t = 240$  when  $p = 0.1$  and  $q = 0.1$ . A few fluctuations in stellar surface density, indicating ring-shaped patterns in the light distribution, are superposed on the initial profile. Colors of the curves represent different time. On both panels, blue, orange, yellow, purple, green, light blue, and dark red correspond to  $t = 0, 40, 80, 120, 160, 200,$  and  $240$ , respectively. On the right panel, curves, except the blue one, are shifted downwards by one unit successively to give a clear view.

sen in our model. One difference is that their scale length goes to infinity at  $p/q = 1$ , while our scale length does that at a  $p/q$  ratio greater than 1. However, this difference fades away when  $d$  in our model goes to 0, as a very small  $d$  makes the scale length go to infinite at a  $p/q$  ratio very close to 1. The derivation of the formula  $0.5\lambda/(q - p)$  in their model also assumes a small  $d$ .

The disc scale lengths are also affected by the model disc edge  $R$ . Default models use an  $R$  of 15 kpc and an annulus width  $d$  of 1 kpc. If we want to analyze a larger galactic disc with an  $R$  of 30 kpc, there are two basic ways to deal with it. On one hand, we can assume that the mechanism responsible for the stellar scattering scales with the model disc edge. As increasing  $R$  to 30 kpc, we also enlarge the annulus width  $d$  to 2 kpc, leaving the number of annulus  $N$  unchanged. On the other hand, one can assume that the stellar scattering is caused by a process unaffected by the global properties of the disc. In this case, we keep the annulus width  $d$  as 1 kpc, but increases  $N$  to 30.

Figure 16 shows the scale length  $h$  as a function of  $p/q$  for  $R = 15, 30, 60$  kpc with various choices of  $d$ . Curves with the same  $R/d$ , i.e. the number of annulus  $N$ , overlap perfectly. This indicates that as  $d$  scales with the model disc edge  $R$ , the scale length  $h$  also scales with the model disc edge  $R$ . When keeping the annulus width  $d$  as 1 kpc, increasing  $R$  from 15 kpc to 30 kpc, and then to 60 kpc, makes the scale length  $h$  go up at any given  $p/q$ , i.e., as the curves go from black to red and then to blue. In this case, the scale length changes are highly sensitive to the value of  $p/q$ . For example, from  $R = 15$  kpc to  $R = 30$  kpc, the scale length increases at  $p/q = 0.5, 0.75, 1,$  and  $1.1$  are 8.46%, 25.1%, 97.0%, and 208.8%, respectively. As

$p/q$  goes up, the increase surges quickly. Particularly, at  $p/q = 1$ , doubling  $R$  gives a scale length increase of about 100%. Even if  $d$  does not scale with the model disc edge  $R$ , the scale length  $h$  will roughly scale with the model disc edge  $R$  as long as  $p/q \approx 1$ .

The observation of real galactic discs shows that the exponential scale length of spiral galaxies increases with the total stellar mass in the disc (Jaffé et al. 2018; Demers et al. 2019). Particularly, Figure 4 of Demers et al. (2019) shows that the disc scale length roughly doubles when the stellar mass goes from  $10^{10.0}M_{\odot}$  to  $10^{10.9}M_{\odot}$ . If we assume that the stellar mass is proportional to the cube of the model disc edge, a mass change from  $10^{10.0}M_{\odot}$  to  $10^{10.9}M_{\odot}$  corresponds to a twofold increase in the model disc edge. Hence, the observed disc scale length approximately scales with the model disc edge. This agrees with the results from our model if the stellar orbital shifts caused by the scattering are treated as proportional to the model disc edge, or if the shifts are unrelated to the model disc edge but the radial scattering has little bias, i.e.  $p/q \approx 1$ .

#### 4.4 Time-dependent scattering probabilities

So far, we have treated  $p$  and  $q$  as two constants in the Markov chain model. As galaxy discs evolve and consume their gas, large clumps, stochastic spiral waves and other scattering centers generally become less prevalent or smaller. Thus, the assumption of constant scattering for gigayears is not realistic in most cases. There are many possible pathways for the evolution of the populations of scattering centers. In this subsection, we consider some sim-

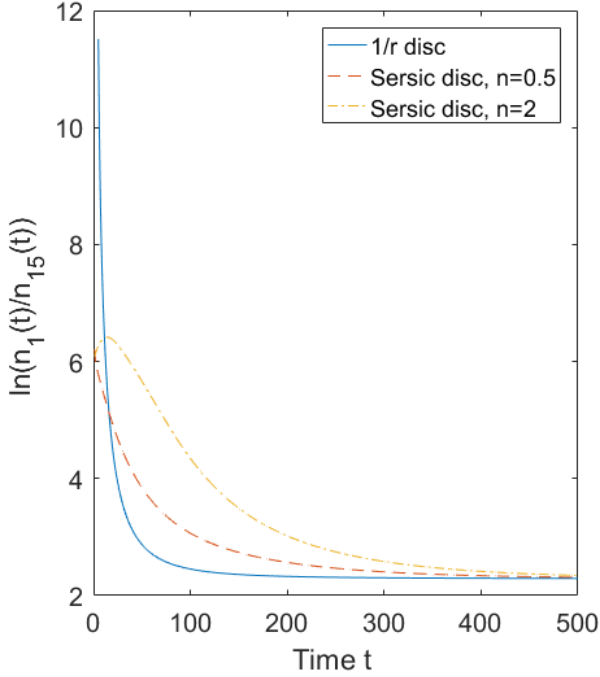


**Figure 11.** Time evolution of  $n_1(t)/n_{15}(t)$  for different initial stellar distributions, when  $p = q = 0.1$ . The blue solid curve, the orange dashed curve, and the yellow dash dotted curve correspond to initial distributions shown on Figure 1, 9, and 10, respectively.

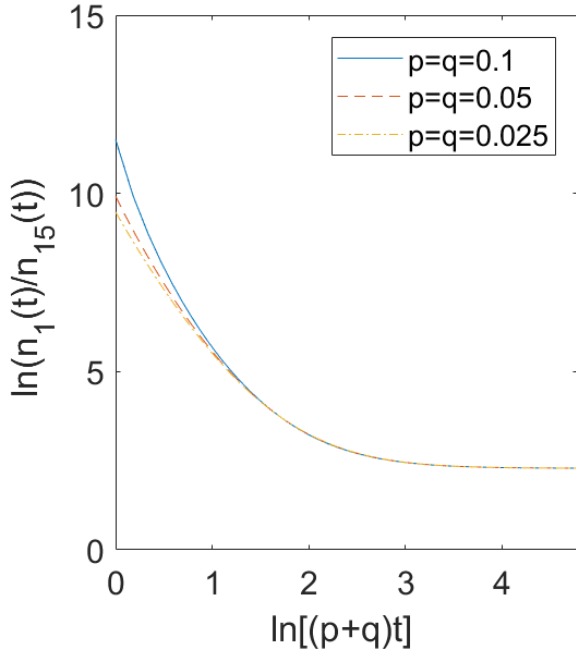


**Figure 12.** Time evolution of  $n_1(t)/n_{15}(t)$  starting from the  $1/r$  disc for different magnitudes of  $p$  and  $q$ . The blue solid curve, the orange dashed curve, and the yellow dash dotted curve correspond to  $p = q = 0.1$ ,  $p = q = 0.05$ , and  $p = q = 0.025$ , respectively.  $\ln[(p + q)t]$  is used for the horizontal axis, where the time  $t$  is in unit of the number of timesteps.

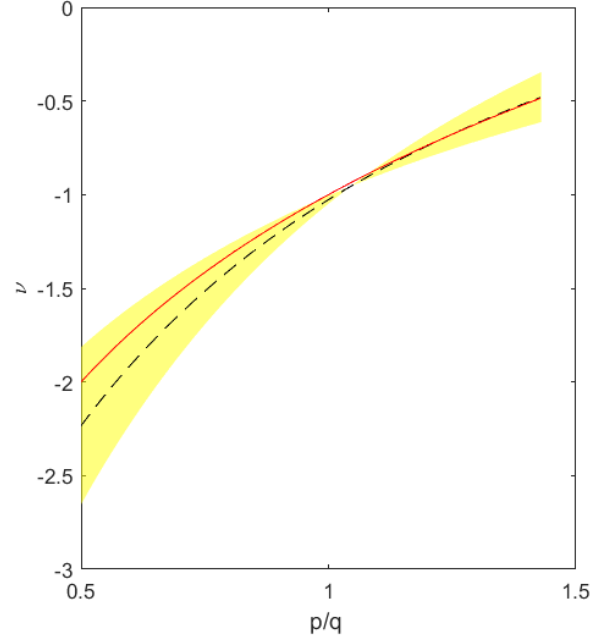


**Figure 13.** The power law fitting result of the quasi-stationary surface density profile at the disc center. The best fitting exponent  $\nu$  is a function of  $p/q$ . The black dashed curve shows the best fitting exponent  $\nu$  using surface density profile at  $r < 3$  kpc. The yellow region indicates the uncertainty in the fitting results. The uncertainty comes from two parts: the standard error of regression coefficients and the model error of using surface density profile at  $r < 3$  kpc. The latter is estimated by slightly altering the radial interval of the fitting. The red solid curve shows the values of  $\nu$  estimated by Equation 15.

ple scenarios when  $p$  and  $q$  decline with time, to illustrate some consequences when scattering in the disc weakens.

When  $p$  and  $q$  are functions of time, we replace  $p$ ,  $q$ , and the matrix  $P$  in Equation 1 with  $p(t)$ ,  $q(t)$  and  $P(t)$ , and Equation 2 becomes

$$\pi(t + 1) = \pi(t)P(t). \quad (16)$$

Here we assume that  $p(t)$  and  $q(t)$  decay exponentially with time and share the same decay rate. With this choice, the  $p(t)/q(t)$  ratio is independent of time and the quasi-stationary distribution is determined by  $p(0)$  and  $q(0)$ . In these discrete models we achieve the exponential decay by setting  $p(t)$  and  $q(t)$  as follows:

$$\begin{cases} p(t) = p(0) \times \gamma^t, \\ q(t) = q(0) \times \gamma^t, \end{cases} \quad (17)$$

where  $\gamma$  is a constant that controls the decay rate.

To study the effect of the time decay of  $p(t)$  and  $q(t)$ , we start the model using the Sérsic profile of the index  $n = 2$ , which has been shown in Section 3.3. With the choice of  $p(0) = 0.1$ ,  $q(0) = 0.1$  and  $\gamma = 0.99$ , the stellar profile evolution from  $t = 0$  to  $t = 500$  is illustrated in Figure 17. In the figure, the profile difference between  $t = 240$  and  $t = 500$  is very small, indicating that the profile evolution ceases at  $t = 500$ . When comparing this figure with Figure 10, the changes of the star number at 1 kpc show that the time-dependent model evolves more slowly from  $t = 0$  to  $t = 240$  and that the profile reached at  $t = 500$  is close to that at  $t = 120$  in the time-independent

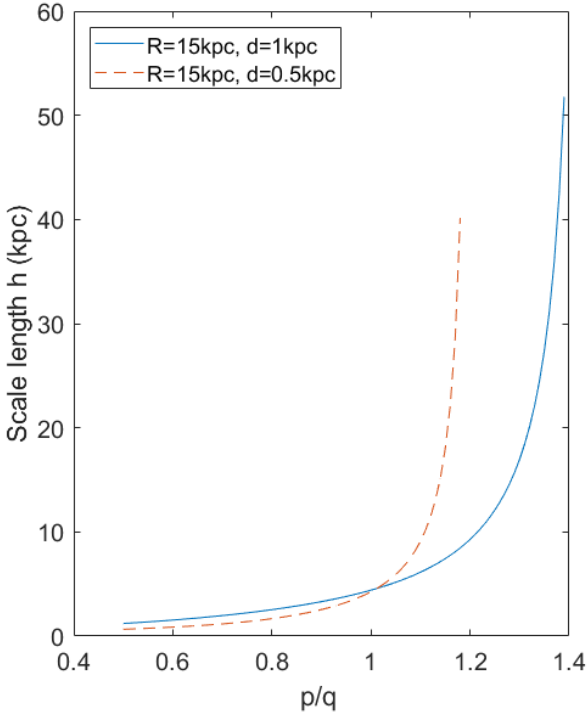


**Figure 14.** The quasi-stationary scale length as a function of  $p/q$  for  $R = 15$  kpc. The solid blue curve and the dashed orange curve correspond to the annulus width  $d = 1$  kpc and  $0.5$  kpc, respectively. The exponential scale lengths are measured from 6 kpc to 10 kpc using linear fits.

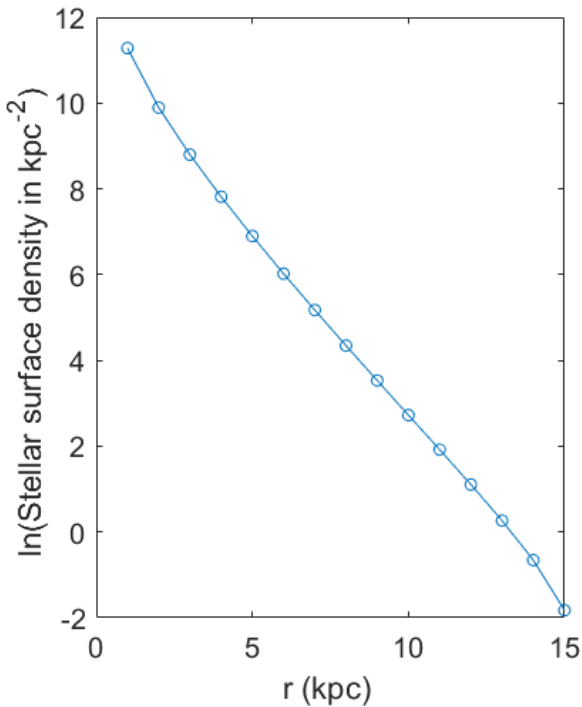


**Figure 15.** The quasi-stationary stellar surface density for  $p/q = 0.5$ , when  $R = 15$  kpc and  $d = 1$  kpc.

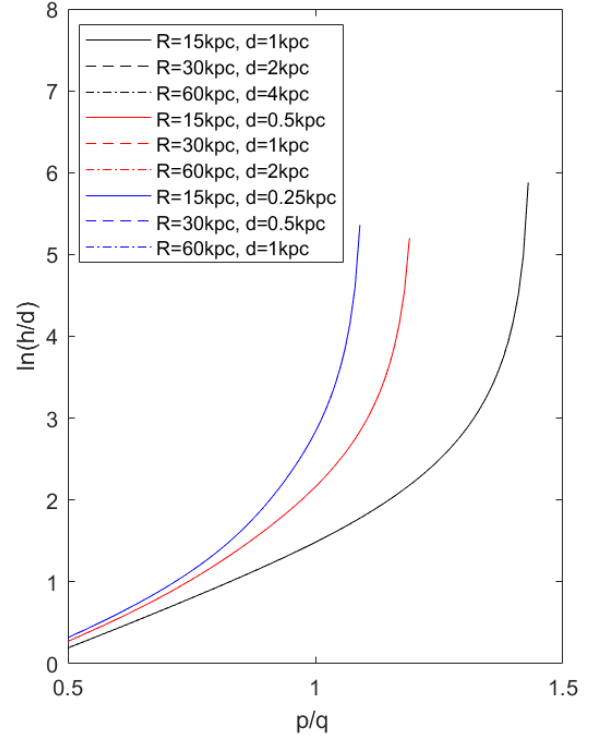


**Figure 16.** The quasi-stationary scale length  $h$  as a function of  $p/q$  for  $R = 15, 30, 60$  kpc with various choices of  $d$ . Curves with the same color share the same  $R/d$  ratio. To better present the curves,  $\ln(h/d)$  is plotted on the vertical axis, instead of  $h$ . In this way, curves with the same color overlap. Nine curves are reduced to three curves, as shown in the figure. For  $R = 30$  and  $60$  kpc, the exponential scale lengths are measured from 13 kpc to 17 kpc and from 26 kpc to 34 kpc, respectively.

model. This suggests that the  $\gamma = 0.99$  model cannot converge to the quasi-stationary distribution corresponding to  $p/q = 1$ .

To better illustrate the profile changes with time, the solid blue curve and the black dashed curve in Figure 18 show  $n_1(t)/n_{15}(t)$  from  $t = 0$  to  $t = 750$  for the  $\gamma = 0.99$  model and the time-independent model, respectively.  $n_1(t)/n_{15}(t)$  in the  $\gamma = 0.99$  model converges to 78.62, much greater than the quasi-stationary ratio of 9.87. After  $t = 240$  in the  $\gamma = 0.99$  model,  $p(t)$  and  $q(t)$  are less than 0.01 due to the exponential time decay. Such small scattering probabilities are unable to make conspicuous changes in the stellar distribution. As a result, the profile evolution gradually stops at an intermediate state on the way toward the quasi-stationary state. From the right panel of Figure 10, one can see that the profile evolution is accompanied by the increase in disk scale length. The final distribution reached by the  $\gamma = 0.99$  model gives an exponential scale length of 2.37 kpc measured from 6 kpc to 10 kpc. This is much smaller than the quasi-stationary scale length of 4.41 kpc, consistent with the claim that the final distribution is an intermediate state on the way toward the quasi-stationary state.

If  $\gamma = 0.999$ , i.e. a slower decay than  $\gamma = 0.99$ , the time evolution of  $n_1(t)/n_{15}(t)$  is presented by the red dot dashed curve in Figure 18.  $n_1(t)/n_{15}(t)$  at  $t = 750$  is very close to that of the time-independent model. In this case, the disc is able to evolve to the quasi-stationary distribution before  $p$  and  $q$  become too small to modify the profile.

In summary, when  $p(t)$  and  $q(t)$  decay exponentially with the



same decay rate, the profile still evolves towards the quasi-stationary distribution, but may freeze at an intermediate stage before reaching it. How far the profile can go on the way to the quasi-stationary distribution depends on the decay rate. Thus, in galaxy discs the ratio of the scattering time to the timescale for the evolution of the scattering centers is an important parameter, e.g., in determining the scale length, and how much of the disc reaches a quasi-steady profile.

#### 4.5 Radial-dependent scattering probabilities

In the real world, scattering centers will not generally be distributed completely uniformly, so in this subsection, we briefly consider some examples where  $p$  and  $q$  are radially dependent. To simplify the problem, we assume here that local scattering does not have radial bias, i.e.  $p_i = q_i$  for all the  $i$ . We also assume that  $p$  and  $q$  do not vary with time.

We begin with the situation where scattering probabilities are the same except for one annulus. The left panel of Figure 19 shows  $t = 2000$  stellar profiles where the scattering probabilities at the 7th annulus are different than the rest of the disc. The quasi-stationary state is reached at  $t = 2000$ , so we can treat the distributions reflected by these curves as the quasi-stationary distributions. When  $q_7 = 0.08$  is less than other  $q_i$  of 0.10, the lower scattering probability at the 7th annulus translates to a lower move-out rate. As a result, stars accumulate at the 7th annulus and the quasi-stationary distribution exhibits a bump there. If  $q_7 = 0.12$  is greater than other  $q_i$  of 0.10, stars at the 7th annulus are diffused and the distribution shows a pit.

The right panel of Figure 19 shows an instance if the scattering probabilities are random values selected from an interval. The resultant quasi-stationary profile has bumps and pits, so it does not follow an exponential distribution. However, if one disregards the fluctuations, it does exhibit a trend of an exponential decay with radius. These examples suffice to show that while moderate radial variations can leave an imprint, they do not disrupt the tendency of scattering to evolve toward the exponential profile.

#### 4.6 Scattering probabilities dependent on both time and radius

In this subsection, we go a little further and discuss stellar profiles where  $p$  and  $q$  vary with both time and radius.

Figure 20 shows stellar profiles where  $p_i$  are randomly selected from the interval of [0.8, 1.2] every 10 timesteps and  $q_i = p_i$  at every radius. In Section 3.1, we show that quasi-stationary distributions are determined by values of  $p$  and  $q$ . Here, as values of  $p$  and  $q$  change with time, the quasi-stationary distribution also varies every 10 timesteps. In other words, the profile evolution will no longer converge to a single distribution.

From the previous subsection, we know that quasi-stationary distributions of randomly selected  $p_i$  and  $q_i$  have a trend of exponential decay with superposed fluctuations. Curves in Figure 20 show the same feature as expected. This confirms the robustness of the scattering model, i.e. scattering always generates an exponential trend in the stellar profile, even if scattering probabilities have moderate radial and time dependence.

#### 4.7 Connecting the model to specific scattering mechanisms

As mentioned in the introduction, the stellar scattering in the radial direction can occur in many processes of different nature. In this

subsection, we focus on the stellar scattering caused by massive clumps in the disc, and discuss the connection between properties of clumps and parameters of the Markov chain model. The scattering owing to other mechanisms may be connected to the Markov chain model using a similar approach.

Key parameters used in the Markov chain model are the model disc edge  $R$ , the annulus width  $d$ , and the scattering probabilities  $p$  and  $q$ . We will discuss these parameters one by one, except  $R$ , which is not directly related to properties of clumps.

When the scattering is due to clumps, orbital changes of stars are caused by the gravitational force of clumps during star-clump encounters. The mass of a clump determines the size of the clump neighbourhood in which the attractive force from the clump can alter stellar motions. It also controls the amplitude of orbital shifts of incoming stars. Stellar orbits in Paper I indicate that encounters involving a clump of  $7.3 \times 10^6 M_\odot$  can lead to a stellar radial change of about 1 kpc. With respect to this clump mass, the annulus width  $d$  can be chosen as 1 kpc so that the scattering from an annulus to adjacent annuli in the Markov chain model mimics the effect of clump-star encounters. If the clump mass is larger (or smaller) than  $7.3 \times 10^6 M_\odot$ ,  $d$  should be increased (or decreased) accordingly to match the amplitude of orbital changes.

The magnitude of scattering probabilities  $p$  and  $q$  in a radial bin can be connected to the clump number density at that galactic radius. A higher clump number density produces more star-clump encounters during a given time period and gives stars a higher chance to move inwards or outwards. The clump number density in the simulations of Paper I roughly corresponds to a scattering probability of 0.05 during 100 Myr. Paper I shows that the clump density gradient affects the scattering bias in the radial direction. This indicates that the clump density gradient can be employed to determine the  $p/q$  ratio. A clump profile with a steep gradient gives an inwards scattering bias, i.e.  $p/q < 1$ , and a shallow gradient leads to an outwards scattering bias, i.e.  $p/q > 1$ . In short, the clump density and the clump density gradient at a galactic radius determine  $p$  and  $q$  in that annulus.

From the discussion in the previous paragraph, it is not hard to see that scattering by clumps is location-dependent. For a given clump density profile, the density and the density gradient of clumps usually is not the same at different galactic radius  $r$ . Therefore,  $p$  and  $q$  are usually functions of  $r$ . In this paper, we discussed only briefly the effect of a radial dependence of  $p$  and  $q$ . This seems to be a good topic to investigate in the future. The connection between clump profile and the  $(p, q)$  pair also suggests that different clump density profiles can lead to distinct profile evolution paths. When an exponential profile is reached, the scale length  $h$  may not be the same for different clump profiles.

Last but not least, the scattering caused by clumps can also be time-dependent. The GADGET-2 simulation in Paper I showed that the frequency of clump-star encounters decline in a long term, indicating that the scattering process weakens with time. To deal with this,  $p$  and  $q$  in the Markov chain model can be written as  $p(t)$  and  $q(t)$  as we did in Section 4.4. However, the time decay of  $p(t)$  and  $q(t)$  may not be exponential, so Equation 17 should not be directly used. To model  $p$  and  $q$  as a function of time and make it consistent with the GADGET-2 simulation, additional work is needed.

In sum, the Markov chain model introduced in the paper can be treated as a general template to study stellar profile evolution. It is capable of connecting to scattering mechanisms with different nature and parameters in the model can be tweaked based on properties of a mechanism.

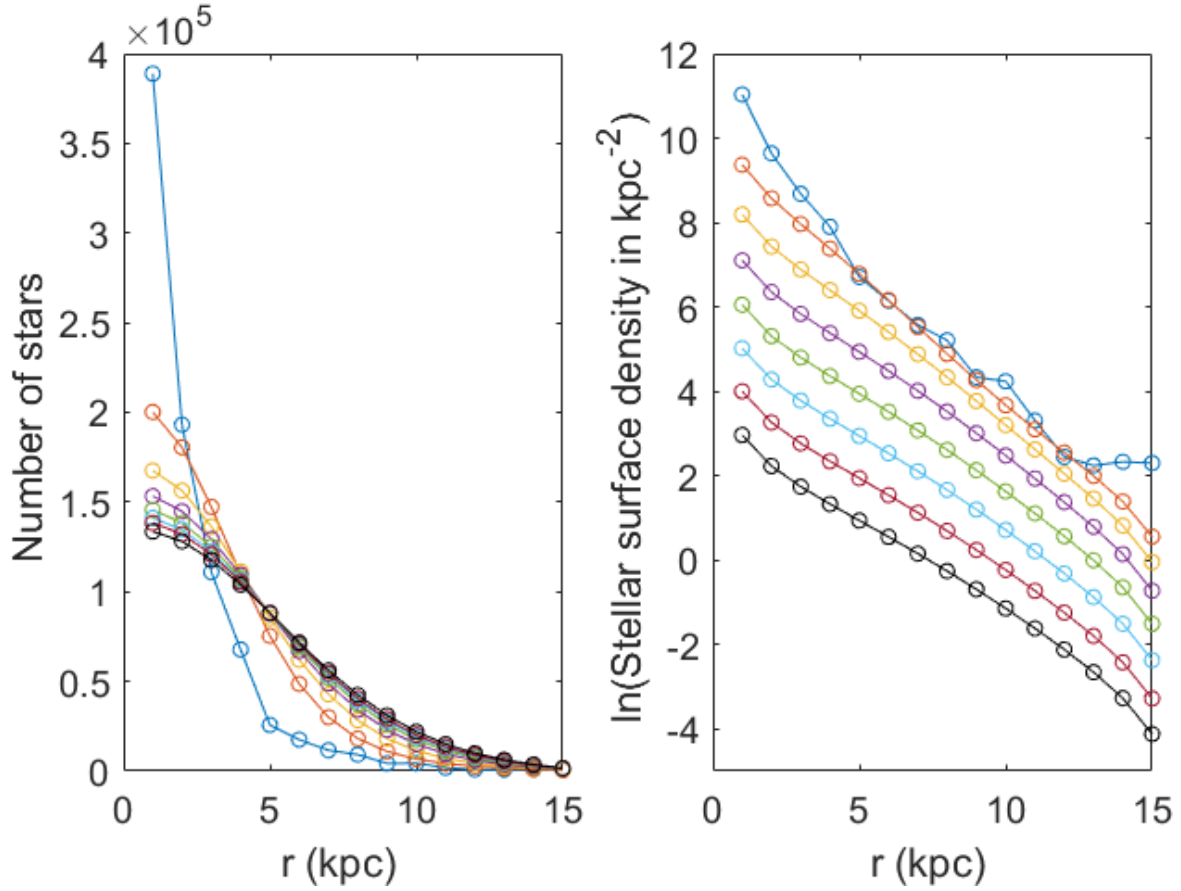


**Figure 17.** An example of stellar profile evolution when  $p(t)$  and  $q(t)$  decay exponentially with time. The initial stellar distribution in this figure is the same as that in Figure 10. Colors of the curves represent different time in the same way as Figure 10, except the black color, which corresponds to  $t = 500$ . On the right panel, curves, except the blue one, are shifted downwards by one unit successively to give a clear view. Parameters used in this example are  $p(0) = q(0) = 0.1$ ,  $\gamma = 0.99$ ,  $R = 15$  kpc,  $d = 1$  kpc.

## 5 SUMMARY

The Markov chain model introduced in this paper shows that radial scattering of stars with location-independent outwards and inwards scattering probabilities,  $p$  and  $q$ , leads to a quasi-stationary stellar distribution with a near-exponential shape. In this model, an inwards scattering bias, i.e.  $p < q$ , is not required. When no bias or a slight outwards bias is present, the stellar profile also evolves towards a near-exponential. This potentially allows this model to build up a stronger connection between the exponential disc formation and many scattering mechanisms, compared with the stochastic models in Elmegreen & Struck (2016), which assume an inward bias. Although stars in the Markov chain model can escape from the galaxy at the edge of the disc, practical initial conditions give rise to only a small star loss, usually less than 10%, before the disc becomes exponential, unless a large outwards scattering bias is chosen.

The exact shape and the scale length  $h$  of the quasi-stationary distribution depend on the  $p/q$  ratio, the galactic disc radius  $R$ , and the radial bin size  $d$ , but do not rely on the initial profile of stars. When  $p/q$  goes from a value less than 1 to a value greater than 1, the quasi-stationary scale length increases with a growing rate. For fixed values of  $p/q$  and  $d$ , the expansion in  $R$  always causes an increase in  $h$ , but the magnitude of the increase is related to  $p/q$ . When the disc radius  $R$  doubles, the scale length  $h$  will double if  $p/q \approx 1$  or if

the radial bin size  $d$  doubles with  $R$ . This scaling relation between  $R$  and  $h$  qualitatively agrees with results from observations (Demers et al. 2019). Given  $R$ , the variation in quasi-stationary scale length due to a fixed change in the radial scattering bias  $p/q$  becomes less as  $d$  increases.

The time it takes to converge to the quasi-stationary distribution depends on the initial stellar profile and the magnitudes of  $p$  and  $q$ . An initial profile far from the quasi-stationary distribution or small magnitudes of  $p$  and  $q$  lead to a long time of convergence. If the magnitudes of  $p$  and  $q$  decay with time, profile evolution can stop at an intermediate stage, failing to get to the presumed quasi-stationary state. As the radial profile change is very rapid at the beginning of a Markov chain run, the intermediate stage may have already reached a near-exponential shape, although different from that of the quasi-stationary state.

Most of the results of this paper have been derived in the context of constant or near constant scattering probabilities  $p, q$  across the model disc, though some spatial and temporal variations were considered in Section 4. It was shown that bumps and dips formed with spatially dependent scattering probabilities, could persist for some time. This raises the possibility that surface density profiles could be tuned to a variety of persistent forms by specific gradients in the scattering probabilities, which could result from gradients in the number or masses of the scattering centers. However, we note

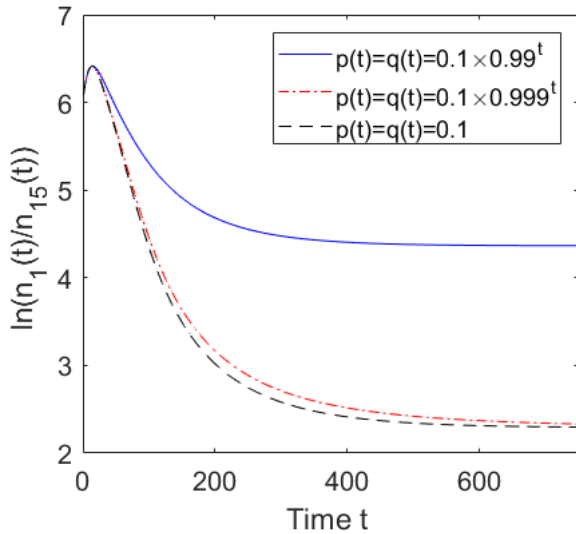


**Figure 18.** Time evolution of  $n_1(t)/n_{15}(t)$  in models with different  $\gamma$  values. The solid blue curve, the dot dashed red curve, and the dashed black curve correspond to  $\gamma = 0.99, 0.999$ , and  $1$ , respectively. Other parameters and the initial stellar distribution in these models are the same as the example in Figure 17.

that the evolution of lumps and dips is inherently self-limiting, rather than self-reinforcing. E.g., in a zone with low scattering probabilities, the excess influx from adjacent zones would build a lump, but the excess density in the lump would increase the outflow from that zone until the scattering fluxes balance. Moreover, if stellar scatterings are caused by massive scattering centers, the distribution of scattering centers is itself likely to be subject to self-regulation. For example, a region with small or few scattering centers, would increase its surface density from an unbalanced inflow, which can lead to enhanced local gravitational instability and the formation of new, massive scattering clumps. The specific timescales are important, and non-exponential profiles may get frozen in if self-regulating processes are slow, as discussed above. The complexities of these issues are beyond the scope of the present paper, but merit further study.

## DATA AVAILABILITY

The data used in this article will be shared on request to the corresponding author.

## REFERENCES

- Andredakis Y. C., Peletier R. F., Balcells M., 1995, *MNRAS*, **275**, 874  
 Bakos J., I. T., Pohlen M., 2008, *ApJ*, **683**, L103  
 Boroson T., 1981, *ApJS*, **46**, 177  
 Bouquin A. Y. K., et al., 2018, *ApJS*, **234**, 18  
 Bournaud F., Elmegreen B. G., Elmegreen D. M., 2007, *ApJ*, **670**, 237  
 Bowler R. A. A., Dunlop J. S., McLure R. J., McLeod D. J., 2017, *MNRAS*, **466**, 3612  
 Bustard C., Zweibel E. G., D’Onghia E., 2016, *ApJ*, **819**, 29  
 Daniel K. J., Wyse R. F. G., 2018, *MNRAS*, **476**, 1561  
 Debattista V. P., Mayer L., Carollo C. M., Moore B., Wadsley J., Quinn T., 2006, *ApJ*, **645**, 209

- Demers M. L., Parker L. C., Roberts I. D., 2019, *MNRAS*, **489**, 2216  
 Elmegreen B. G., Struck C., 2013, *ApJ*, **775**, L35  
 Elmegreen B. G., Struck C., 2016, *ApJ*, **830**, 115  
 Elmegreen B. G., Elmegreen D. M., Vollbach D. R., Foster E. R., Ferguson T. E., 2005, *ApJ*, **634**, 101  
 Elmegreen B. G., Struck C., Hunter D. A., 2014, *ApJ*, **796**, 110  
 Erwin P., Beckman J. E., Pohlen M., 2005, *ApJ*, **626**, L81  
 Freeman K. C., 1970, *ApJ*, **160**, 811  
 Herpich J., Tremaine S., Rix H.-W., 2017, *MNRAS*, **467**, 5022  
 Herrmann K. A., Hunter D. A., Elmegreen B. G., 2013, *AJ*, **146**, 104  
 Hobbs A., Read J., Power C., Cole D., 2013, *MNRAS*, **434**, 1849  
 Hohl F., 1971, *ApJ*, **168**, 343  
 Ichikawa S. I., Wakamatsu K. I., Okamura S., 1986, *ApJS*, **60**, 475  
 Jaffé Y. L., et al., 2018, *MNRAS*, **476**, 4753  
 Law D. R., Steidel C. C., Shapley A. E., Nagy S. R., Reddy N. A., Erb D. K., 2012, *ApJ*, **745**, 85  
 Li J.-Y., Jiang Z.-B., Liu Y., Wang Y., 2013, *Research in Astronomy and Astrophysics*, **13**, 921  
 Lin D. N. C., Pringle J. E., 1987, *ApJ*, **320**, L87  
 Marr J. H., 2020, *Galaxies*, **8**, 12  
 Normandeau M., Taylor A. R., Dewdney P. E., 1996, *Nature*, **380**, 687  
 Patrício V., et al., 2016, *MNRAS*, **456**, 4191  
 Patterson R. J., Thuan T. X., 1996, *ApJS*, **107**, 103  
 Pavel M. D., Clemens D. P., 2012, *ApJ*, **760**, 150  
 Peñarrubia J., McConnachie A., Babul A., 2006, *ApJ*, **650**, L33  
 Roškar R., Debattista V. P., Stinson G. S., Quinn T. R., Kaufmann T., Wadsley J., 2008, *ApJ*, **675**, L65  
 Sellwood J. A., Binney J. J., 2002, *MNRAS*, **336**, 785  
 Shibuya T., Ouchi M., Kubo M., Harikane Y., 2016, *ApJ*, **821**, 72  
 Simard L., Mendel J. T., Patton D. R., Ellison S. L., McConnachie A. W., 2011, *ApJS*, **196**, 11  
 Struck C., Elmegreen B. G., 2017, *MNRAS*, **469**, 1157  
 Struck C., Elmegreen B. G., 2018, *ApJ*, **868**, L15  
 Struck C., Elmegreen B. G., 2019, *MNRAS*, **489**, 5919  
 Vera-Ciro C., D’Onghia E., Navarro J., Abadi M., 2014, *ApJ*, **794**, 173  
 Wang E., Lilly S. J., 2022, *ApJ*, **927**, 217  
 Wu J., Struck C., D’Onghia E., Elmegreen B. G., 2020, *MNRAS*, **499**, 2672  
 Wu J., Struck C., Elmegreen B. G., D’Onghia E., 2022, *MNRAS*, **517**, 4417  
 de Jong R. S., 1996, *A&A*, **313**, 45

This paper has been typeset from a  $\text{\TeX}/\text{\LaTeX}$  file prepared by the author.

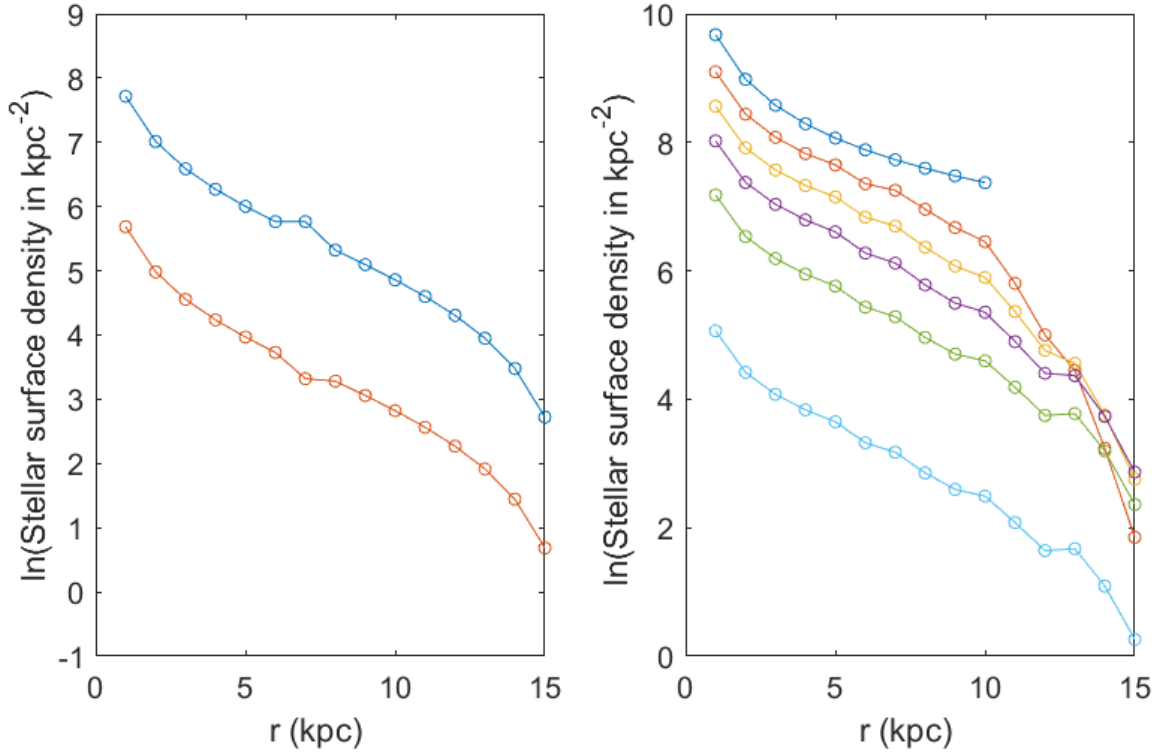


**Figure 19.** Stellar profiles when  $p$  and  $q$  are radially dependent. The left panel shows surface density profiles where  $p_i = q_i = 0.1$  except for  $i = 7$ . The top curve in this panel corresponds to  $t = 2000$  (blue) with  $p_7 = q_7 = 0.08$ . The bottom curve in this panel corresponds to  $t = 2000$  (orange) with  $p_7 = q_7 = 0.12$ . The bottom curve is shifted downwards by two units to avoid overlapping with the top one. For both curves, the initial stellar distribution is the same as that in Figure 1. The right panel shows an instance of surface profile evolution, if  $p_i$  are randomly selected in the interval of  $[0.8, 1.2]$  and  $q_i = p_i$ . Here  $p_i$  and  $q_i$  do not vary with time. In this panel, the curves from top to bottom correspond to  $t = 0$  (blue), 20 (orange), 40 (yellow), 80 (purple), 400 (green), and 2000 (light blue), respectively. Curves, except the top one, are shifted downwards by 0.5 unit successively to give a clear view. The large separation between the green curve and the light blue one is caused by star loss at the edge of the disc.

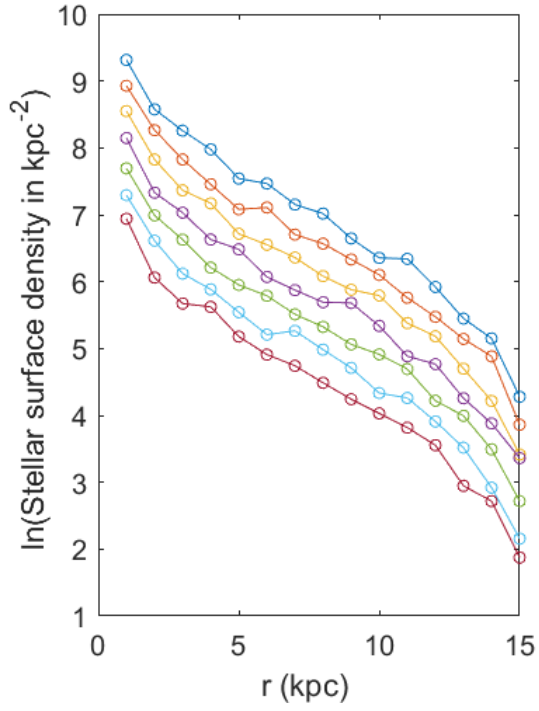


**Figure 20.** Stellar profile evolution of an instance where  $p$  and  $q$  vary with both time and radius. Here time is divided into periods of 10 timesteps. At the beginning of each period,  $p_i$  are randomly selected in the interval of  $[0.8, 1.2]$  and stay unchanged within the period.  $q_i$  is chosen to be equal to  $p_i$  at every radius all the time. The curves from top to bottom correspond to  $t = 400$  (blue), 800 (orange), 1200 (yellow), 1600 (purple), 2000 (green), and 2400 (light blue), and 2800 (dark red), respectively. The initial stellar distribution is the same as that in Figure 1.